hydrology

MDPI

Article

Flood Susceptibility Mapping: Scenario-Based Multi-Criteria Decision-Making Versus Random Forest Model

Mehdi Rahimi [1,2], Bahram Malekmohammadi [1], Mohammad Karimi Firozjaei [3], Reza Kerachian [4] and Farhad Bahmanpouri [5,*]

[1] Graduate Faculty of Environment, University of Tehran, Tehran 1417853111, Iran; rahimi.mehdi@ut.ac.ir (M.R.); malekb@ut.ac.ir (B.M.)
[2] Scientific Research Center, Al-Ayen University, Nasiriyah, Thi-Qar, 64001, Iraq
[3] Collage of Management, University of Tehran, Tehran 1411713114, Iran; mohammad.karimi.f@ut.ac.ir
[4] School of Civil Engineering, College of Engineering, University of Tehran, Tehran 1417613131, Iran; kerachian@ut.ac.ir
[5] Research Institute for Geo-Hydrological Protection, National Research Council (CNR), 06128 Perugia, Italy
* Correspondence: farhadbahmanpouri@cnr.it

Abstract

Floods are among the most destructive natural hazards, posing a significant risk to lives and infrastructure worldwide. Effective flood risk management demands precise, multidimensional approaches. In this direction, the current study aims to evaluate and compare two methods for flood-risk assessment: the scenario-based Ordered Weighted Averaging (OWA) and the data-driven Random Forest (RF) method. To this end, the Great Karun watershed in Iran was chosen due to its complex hydrological and climatic conditions. Hydro-climatic, hydrological, topographic, land-cover datasets, and actual flood observations were applied and analyzed based on fifteen influencing factors recommended by expert opinion. In the OWA approach, while factor weights were determined using the Best-Worst Method, flood-risk maps were produced based on five scenarios: very optimistic, optimistic, intermediate, pessimistic, and very pessimistic. In the RF approach, factor importance index was calculated via the mean decrease impurity algorithm, and the model was trained to generate flood-risk maps. Results showed that distance from rivers and slope were the most influential factors in OWA, while precipitation and flow accumulation dominated in RF. Prediction rate for OWA scenarios ranged from 1.4 to 3.5%, while RF achieved 16.0%, and the Area Under the Curve (AUC) was 0.984. Optimistic scenarios overestimated, and pessimistic scenarios underestimated risk, with the OWA intermediate scenario most closely matching RF results. RF demonstrated superior performance for flood-risk classification, highlighting its applicability for precise flood management. Overall, this study presents a novel comparative framework by integrating scenario-based OWA-BWM and Random Forest approaches to investigate the effects of decision-maker preferences and data-driven learning on flood susceptibility mapping.

Keywords: flood analysis; mapping; multi-criteria decision making; spatial learning; geospatial analysis

Check for updates

Academic Editor: Brunella Bonaccorso

Received: 28 April 2026
Revised: 25 June 2026
Accepted: 8 July 2026
Published: 11 July 2026

Copyright: © 2026 by the authors. Licensee MDPI, Basel, Switzerland. This article is an open access article distributed under the terms and conditions of the Creative Commons Attribution (CC BY) license.

1. Introduction

Flooding is considered one of the most widespread and destructive natural hazards. The exposure of populations and assets to floods, reportedly, has increased dramatically

over the past few decades [1,2]. Since 1985, human settlements worldwide have continuously and at an increasing pace expanded into flood-prone areas [3]. Meanwhile, studies indicate that over the past decade, more than two billion people around the globe have been affected by flood events, accounting for roughly half of all natural-disaster-related fatalities. Floods can also lead to severe post-event consequences that may impact public and community health for an extended period [4–6]. Climate change is considered one of the factors influencing the variations in climatic variables, as it increases the frequency and intensity of extreme climatic hazards and events such as floods [7,8], thereby posing a threat to ecosystem sustainability [9]. Climate change, by increasing global temperatures, has altered precipitation and runoff patterns, leading to a rise in the frequency and intensity of floods in many regions worldwide. Results indicate that by 2050, in numerous areas globally, including Asia, flood events that previously occurred once every 100 years may happen twice as often [10].

In other words, research seriously warns that the intensity of extreme precipitation and floods will increase by the end of the 21st century in all climates; this increase will be particularly severe in regions with more water availability and will be more pronounced during seasonal cycles [11,12]. Although much of the focus is on severe and damaging floods, it should not be forgotten that milder forms of flooding, such as nuisance flooding (shallow and low-depth floods), can also have significant effects on daily life, urban infrastructure, and the quality of life for citizens. Therefore, a more comprehensive understanding of the different dimensions and types of floods, including their economic, social, and environmental impacts, plays an important role in risk and hazard management, the development of preventive policies, and the reduction in community vulnerability to this natural phenomenon [13]. The various forms of floods and the complexity in deeply understanding their mechanisms have necessitated a system approach to flood analysis. Consequently, flood issues are nowadays analyzed not only from a technical and engineering perspective but also through interdisciplinary research and advancements in computer sciences, particularly in artificial intelligence, data analysis, and geographical analysis tools, with an emphasis on flood engineering. The remarkable progress in artificial intelligence, especially machine learning models, as one of the most significant interdisciplinary tools, has played an increasing and practical role in flood risk management. By utilizing effective data such as hydrological, climatic, and topographical factors, new horizons have been opened in data analysis, feature engineering, zoning, identifying occurrence potential, and more accurate flood prediction. This highlights the necessity of shifting towards data-driven flood risk management strategies supported by AI tools [7,14–17]. In this regard, over recent years, the development of novel frameworks for identifying and mapping flood risk, relying on machine learning algorithms and their combination or comparative evaluation with multi-criteria decision analysis methods, has been recognized as an effective step towards enhancing the accuracy of analyses and increasing the interpretability of models [18]. The combination of the power to understand complex environmental interactions and learn hidden patterns within big data, along with the high predictive capabilities of machine learning models, when integrated with flexible decision-making approaches [19], enables a more accurate spatial assessment of flood risk with greater adaptability to environmental conditions and management preferences. Such a particular approach can lead to the production of more comprehensive flood risk maps that are not only based on diverse data but also incorporate uncertainties and associated risks into the decision-making process. These tools and approaches are of particular importance in improving crisis management, reducing the vulnerability of high-risk areas, and moving towards sustainable development in the face of extreme events.

Given the importance of the subject, numerous studies have been conducted in recent years that clearly demonstrate the significant advancements of machine learning models in predicting and mapping flood risk. These studies have well-documented the capability, accuracy, and adaptability of these models in identifying and mapping flood risk [8,19–31]. In the lower Niger River basin (Nigeria), machine learning models using environmental, climatic, and topographic factors achieved effective flood risk mapping. The XGBoost model showed the highest accuracy (91%) and identified river confluence areas as high-risk zones [32]. In another research conducted in the Lanyang Plain (Taiwan), a hybrid RF–SOM model improved flood risk mapping accuracy and enhanced the detection of high and very high-risk areas by up to 30% compared with conventional methods [33]. Based on a novel study, in the Armbagh region (India), a machine learning framework achieved over 80% accuracy in flood risk mapping. SHAP and Boruta analyses identified elevation, rainfall, and distance from rivers as key factors, with 17–18% of the area exposed to high flood risk [34].

In subsequent research conducted in the Ajichay River basin (northwestern Iran), different neural network models were evaluated for flood susceptibility mapping. The results showed that elevation was the most influential factor, and the MLP model with a sigmoid function achieved the best performance with 92.1% AUC accuracy [35]. In a related study conducted in the central-west coast of India, hybrid machine learning models integrating Adabag with different algorithms improved flood susceptibility mapping. The Adabag–Rotation Forest model achieved the highest accuracy (94%), outperforming individual models [36].

In an alternative study, in Kermanshah city (Iran), machine learning models were applied for urban flood risk mapping under limited data conditions. The RF model showed the best performance (AUC-ROC = 99.5%), with distance from channels, land use, and Curve Number identified as the most influential factors [37]. According to the new study conducted in the Abarkuh region (Iran), a hybrid approach integrating machine learning models and ANP–DEMATEL was developed for flood risk assessment. The SVM model achieved the best performance, identifying precipitation, vegetation cover, and stream density as key influencing factors, with 75% of the area classified as high or very high risk [38]. In a study through the Kalvan watershed (Iran), decision tree-based machine learning models were applied for flood susceptibility mapping. The ERT model achieved the best performance (AUC = 0.82), identifying elevation, slope, precipitation, and distance from rivers as key controlling factors [39]. In another investigation carried out in the arid Xinjiang region (China), the RF algorithm was applied for storm flood risk mapping and achieved an accuracy of 83.48%. The results showed that mountainous areas, river downstream plains, and lake surroundings were more flood-prone, with hazard intensity, population density, road density, distance from rivers, and precipitation as key factors [40]. While machine learning models are effective at identifying complex relationships between flood-influencing variables, they often operate on local scales using training data and offer limited direct control over the decision-making process. In contrast, multi-criteria decision-making (MCDA) approaches, such as the Ordered Weighted Averaging (OWA) method, enable a well-considered and flexible evaluation of flood risk across broader spatial analysis levels. OWA, by employing ordered weights and a parametric structure, allows decision-makers to simulate various decision-making approaches within different scenarios, ranging from very pessimistic to very optimistic. This enables an examination of the model's sensitivity to changes in preferences or uncertainty conditions, making OWA a potent tool for scalable and scenario-based analyses in environmental risk management, such as flood mitigation.

In a recent research study conducted in the Dadou River basin (China) for flood risk zonation, three multi-criteria analysis methods such as AHP, TOPSIS, and OWA (with $\alpha = 1$) were employed within a GIS framework. The results indicated that the areas of Luding, Yuexi, and their surroundings exhibit the highest risk levels. The flood risk distribution patterns were similar across all three methods, and validation with historical flood occurrence data confirmed the high accuracy and reliability of the generated maps [41]. In a related deep study conducted in Mazandaran Province, Iran, flood risk maps were prepared using OWA-based GIS analysis with two types of weighting: subjective and combined subjective-objective. The results showed that under fully pessimistic and optimistic strategies, the percentage of flood-prone areas in the "very high" risk class was 14.65% and 100%, respectively. The assessment ratio was consistent at 4.47 and 1.2 for both weighting types [42]. In a subsequent research, flood risk maps were prepared using GIS and the AHP and OWA methods. Nine effective parameters, including elevation, slope, curvature, precipitation, and others, were weighted according to their importance. The results indicated that the area is divided into five zones with risks of very low (13.16%), low (19.16%), medium (23.07%), high (30.31%), and very high (14.30%). The largest area corresponds to the high-risk zones. The OWA method's performance was well demonstrated in this study for generating flood risk maps with more precise delineation of vulnerable areas, providing a suitable basis for management decisions [43].

Based on a new investigation, flood potential was analyzed using the Ordered Weighted Average (OWA) model. In this research, eight criteria were selected as input factors. After initial preprocessing using ArcGIS (10.8.2) software and specialized tools such as the OWA model with three-tier weights including ANDness, ORness, and Tradeoff, modeling was executed. Based on this, flood potential maps for the study area were generated. The results highlighted the effective role of the OWA model in analyzing and determining different levels of flood risk on a spatial scale [44]. The conducted investigations indicate that in flood risk and zonation assessments, determining the degree of influence of various factors plays a crucial role in the accuracy and reliability of the results. This determination can be achieved using two main categories of methods: subjective methods, which are based on expert opinions and human experience and are often applicable when insufficient data is available, and objective methods, which are based on real data and mathematical and statistical models, such as dependence analyses, weighting, and machine learning algorithms. The significance of these methods in flood risk mapping stems from their ability to identify and prioritize factors influencing flood occurrence and intensity, such as topography, land use, precipitation, etc., which directly relates to the accuracy of zonation and management decisions. An intelligent combination of subjective and objective methods can enhance the reliability of risk maps and improve the management of flood prevention and damage reduction, which is one of the main objectives of this research.

The aim of this study is to develop a comprehensive comparative framework for flood susceptibility mapping by integrating a scenario-based multi-criteria decision-making approach and a data-driven machine learning model. Unlike previous studies that mainly focused on comparing conventional GIS-based multi-criteria techniques with machine learning algorithms, this research introduces a novel scenario-based OWA-BWM framework that incorporates different decision-maker risk preferences (from very optimistic to very pessimistic conditions) into flood susceptibility assessment. This capability enables the evaluation of how variations in risk attitudes influence susceptibility patterns and provides a more flexible decision-support framework for flood risk management. In parallel, the Random Forest (RF) algorithm is applied as a data-driven approach to capture complex nonlinear relationships between flood occurrence and environmental conditioning factors using historical flood observations. The novelty of this study lies in

the systematic comparison of expert-driven and data-driven modeling approaches under the same spatial framework, providing new insights into the advantages, limitations, and uncertainty associated with each method. Moreover, to the best of our knowledge, such an integrated scenario-based OWA-BWM and RF comparison has not previously been conducted in the Great Karun watershed. The findings of this study can support more reliable flood susceptibility assessment and assist decision-makers in developing effective flood risk reduction and management strategies. The main research question of this study is whether a data-driven machine learning approach (Random Forest) can outperform a human judgment-based multi-criteria decision-making method (OWA-BWM) in terms of accuracy, robustness, and generalization capability in flood susceptibility mapping at the watershed scale. Accordingly, the main hypothesis of this study is that the Random Forest model, due to its ability to learn complex nonlinear patterns from observational data, provides higher predictive accuracy and better generalization performance compared to the OWA-BWM model, which relies on subjective weighting and scenario-based human decision preferences.

2. Materials and Methods

2.1. Case Study: Great Karun Basin

The Great Karun Basin, as one of the significant sub-basins of the Persian Gulf and Sea of Oman watershed, covers an area of approximately 66,675 km^2 and comprises 10 distinct sub-basins. The Karun River, with its unique characteristics as the longest, most voluminous, and largest river in Iran, plays a fundamental role in supplying the region's hydroelectric power. Topographically, about 74% of this basin consists of mountainous and high-altitude areas, while 25% comprises plains and low-lying lands. This basin encompasses numerous provinces, including Khuzestan, Lorestan, Chaharmahal and Bakhtiari, Kohgiluyeh and Boyer-Ahmad, Markazi, and Isfahan. The extensive climatic diversity across these provinces, ranging from arid to temperate and snowy climates, has resulted in considerable fluctuations in hydro-climatic indicators. Nevertheless, the impacts of human activities, particularly dam construction, have led to changes in the basin's hydrological regime and have reduced its adaptability to natural hazards. These complexities have cemented the key position of the Karun Great Basin in the country's strategic planning. Figure 1 illustrates the geographical coordinates of this region.

2.2. Datasets

In this research, in order to investigate the risk of flooding in the study area, spatial data were classified into four main categories, including climatic data, hydrological data, data related to land cover and properties, and topographic data. The spatial resolution of all layers was considered to be 300 m. To ensure spatial consistency among all conditioning factors, the raster datasets were standardized to a spatial resolution of 300 m using the resampling procedure in ArcGIS. The original high-resolution raster layers were resampled using the Nearest Neighbor method to preserve the original spatial characteristics of the input data.

To generate spatial maps, distance-based methods and reclassification of the digital elevation model were first used to create geomorphological maps. Other spatial layers, including hydrological information, land cover, topographic features, and indices related to water flow and accumulation, were also calculated and processed. For the machine learning model modeling stage, all layers were standardized to enable direct comparison. To extract the flooded areas layer, which occurred globally between the years 2000 and 2018, the Global Flood Database was used and extracted for the study area. The Global

Flood Database includes maps of the extent and temporal distribution of flood events that occurred from 2000 to 2018 [45].

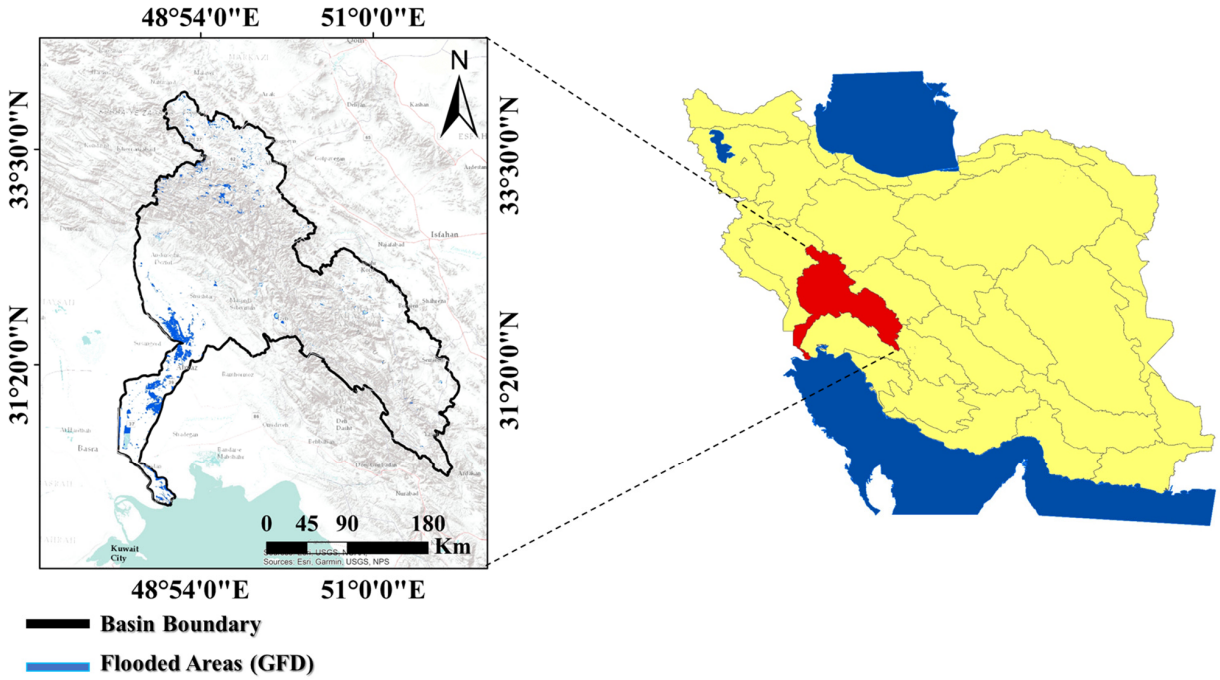


Figure 1. The study area for the current research.

To update and improve the flood inventory dataset, an additional flood extent extraction process was performed using the Normalized Difference Water Index (NDWI) change detection approach in the Google Earth Engine (GEE) platform. Sentinel-3 OLCI images were analyzed before and after the March 2019 flood event to identify newly inundated areas. The NDWI difference between pre-flood and post-flood conditions was calculated, and areas showing significant increases in surface water response (NDWI > 0.1) were classified as newly flooded regions. Consequently, the historical flood inventory was updated from 2000 to 2018 to 2000–2019, providing a more comprehensive target dataset for flood susceptibility modeling. The information obtained from this dataset was classified into two classes: flooded areas and non-flooded/permanent areas. Table 1 shares information concerning the dataset used in the current study.

Table 1. The main data used in this research.

Data	Source (accessed on 28 April 2026)
Precipitation	https://www.irimo.ir/eng/index.php
Temperature	https://www.irimo.ir/eng/index.php
Evapotranspiration	https://www.irimo.ir/eng/index.php
Snow Cover	https://developers.google.com/earth-engine/datasets/catalog/NASA_FLDAS_NOAH01_C_GL_M_V001
Rivers	https://www.moe.gov.ir/?lang=en-us
Vegetation Cover (NDVI)	https://developers.google.com/earth-engine/datasets/catalog/LANDSAT_COMPOSITES_C02_T1_L2_32DAY_NDVI
Land Cover	https://developers.google.com/earth-engine/datasets/catalog/KNTU_LiDARLab_IranLandCover_V1
Soil Class	http://www.swri.ir/en-US/DouranPortal/1/page/Home

Table 1. *Cont.*

Data	Source (accessed on 28 April 2026)
Geology Class	https://gsi.ir/en
Digital Elevation Model (DEM)	https://developers.google.com/earth-engine/datasets/catalog/JAXA_ALOS_AW3D30_V3_2
Flooded Areas	https://developers.google.com/earth-engine/datasets/catalog/GLOBAL_FLOOD_DB_MODIS_EVENTS_V1
Flooded Point (Validation)	www.kwpa.ir, www.wrm.ir

Overall, the flood inventory used in this study covers the period 2000–2019, ensuring a long-term representation of observed flood events. To maintain temporal consistency, all dynamic environmental predictor variables were computed as multi-year averages over the same period using the Google Earth Engine (GEE) platform.

2.3. Effective Criteria on Flooding

The criteria used in this research were divided into four categories: Hydroclimate, Hydrologic, Earth Cover, and Topography to cover all possible factors on the flood susceptibility of the study area. The four categories and their criteria are explained below.

Climate: Climatic conditions are among the fundamental factors controlling flood susceptibility due to their direct influence on the hydrological cycle. In this study, rainfall, air temperature, evapotranspiration, and snow cover were selected to characterize the climatic setting of the study area. Rainfall provides the primary source of water input, whereas temperature regulates snowmelt and evaporation processes. Evapotranspiration governs moisture loss from the land surface, and snow cover acts as a temporary water reservoir whose melting can substantially increase runoff. Considering these variables together enables a more comprehensive representation of climatic variability and its influence on flood susceptibility, thereby improving the robustness of the susceptibility assessment.

Hydrological: Hydrological characteristics play a decisive role in controlling the movement, concentration, and storage of surface water within a watershed. To capture these processes, five hydrological indicators were incorporated into the analysis: distance to rivers, distance to dams, drainage density, stream power index (SPI), and flow accumulation. These variables collectively describe the connectivity of the drainage network, the potential energy of flowing water, and the capacity of the landscape to collect and convey runoff. Their combined evaluation provides valuable insight into the spatial variability of flood susceptibility and supports the identification of locations where runoff is more likely to accumulate and generate flooding.

Earth Cover: Land surface characteristics strongly influence the partitioning of rainfall into infiltration, storage, and surface runoff. To represent these effects, four surface-related variables were incorporated into the analysis: soil type, geological formation, vegetation cover, and land cover. These factors determine the physical properties of the terrain, regulate water infiltration and retention, and modify runoff generation under different environmental conditions. Their combined contribution provides a realistic representation of surface conditions and improves the identification of areas with varying levels of flood susceptibility.

Topography: Terrain configuration is a primary factor governing the direction, velocity, and concentration of overland flow. In this study, topographic conditions were characterized using elevation, slope, the topographic wetness index (TWI), curvature, and the sediment transport index (STI). These variables describe the geometric properties of the landscape and its ability to accumulate, retain, or route water across the watershed. By cap-

turing variations in terrain morphology, they provide essential information for identifying flood-prone locations and enhancing the accuracy of flood susceptibility assessment.

Figure 2, highlights the normalized criteria, standardized according to the magnitude and direction of their influence on flood susceptibility. Figure 3 shows the land cover, soil properties, and geology class of the Great Karun basin. Due to the vastness of this watershed, the high diversity in its earth cover causes the basin's behavior in different areas to vary in terms of water infiltration or its conversion to runoff, exhibiting different behaviors in various regions.

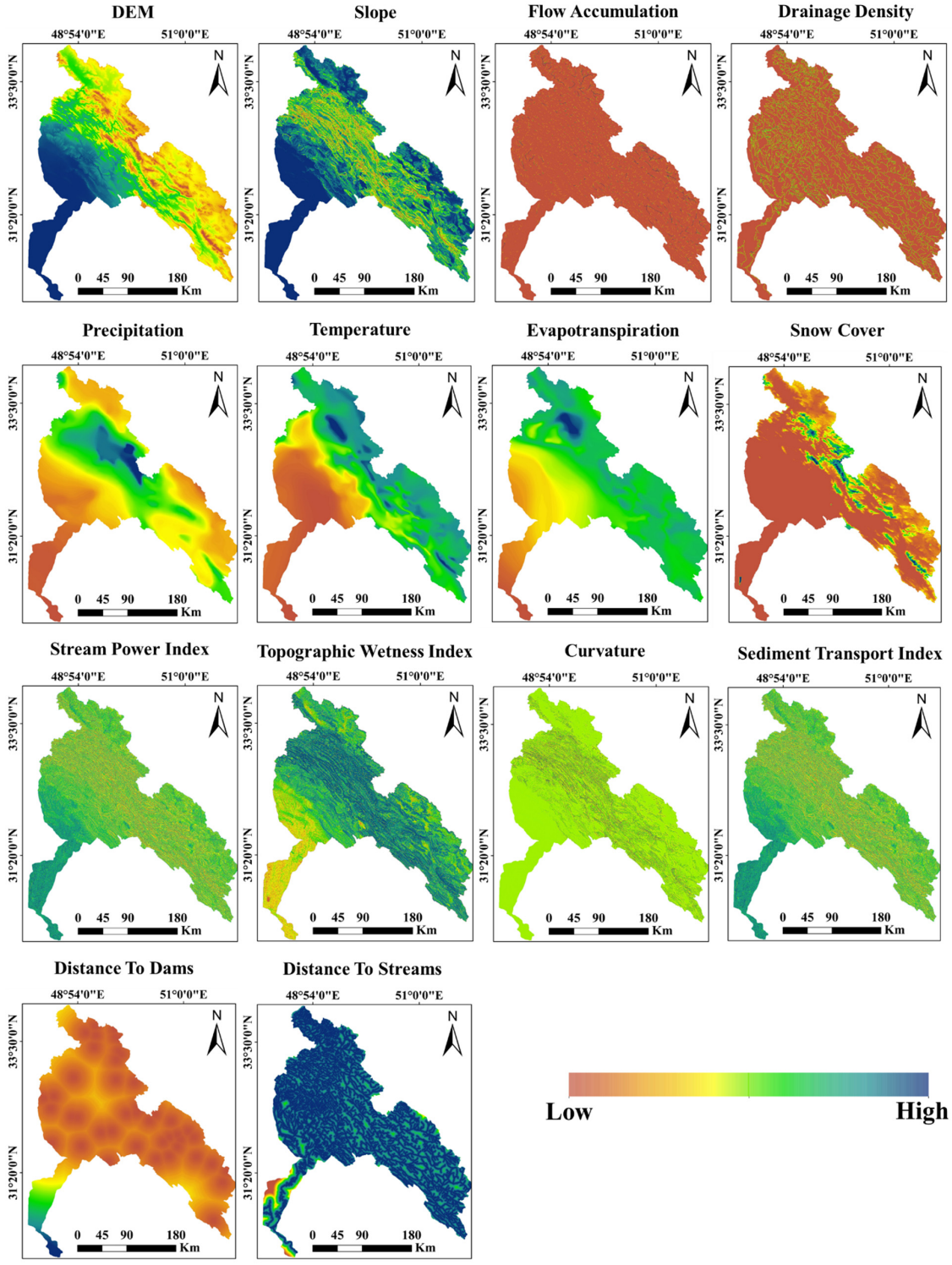


Figure 2. Map of continuous criteria influencing flood susceptibility.

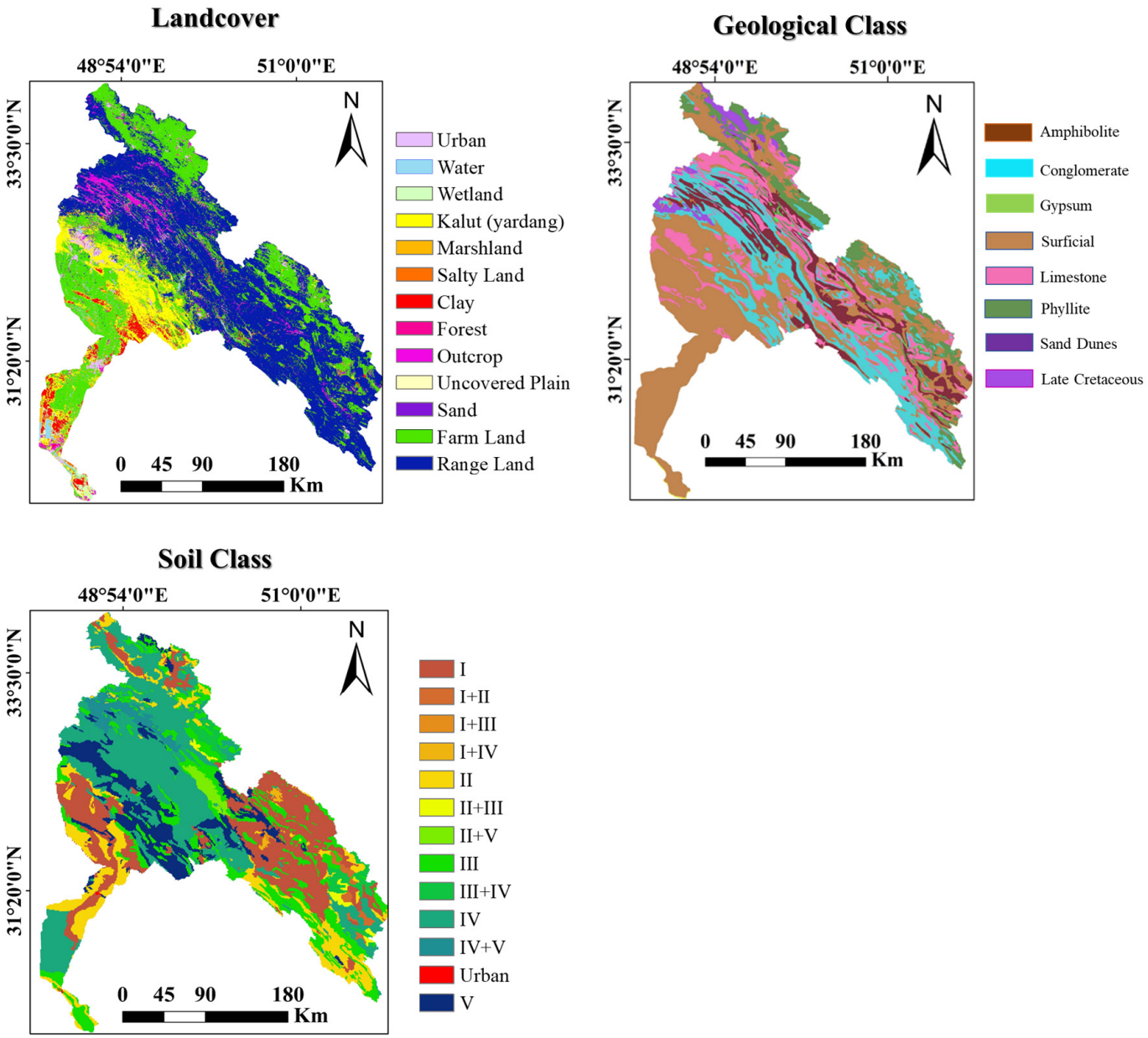


Figure 3. Map of the Earth cover criteria Influencing flood susceptibility.

2.4. Methodology

The schematic of the current research methodology based on the different steps is shown in Figure 4. In the first step, the factors affecting flooding (Table 1) in the study area were identified. This stage involved selecting the indicators and criteria that have the greatest impact on the occurrence and probability of floods, based on climatic, topographic, hydrological, and land cover characteristics. In the second step, using spatial analyses in a GIS environment, the information layers and spatial maps related to each of the effective factors were prepared. These layers were used as input data for two decision-making models: OWA and the RF machine learning model. In the final step, the accuracy of the models and their resulting outputs across different flood risk classes (from very low to very high potential) were comparatively evaluated. This evaluation was conducted with the aim of determining each model's capability in accurately predicting flood-prone areas. Finally, based on the obtained results, the model with the highest accuracy and efficiency was selected as the best method or scenario for flood risk prediction in the region.

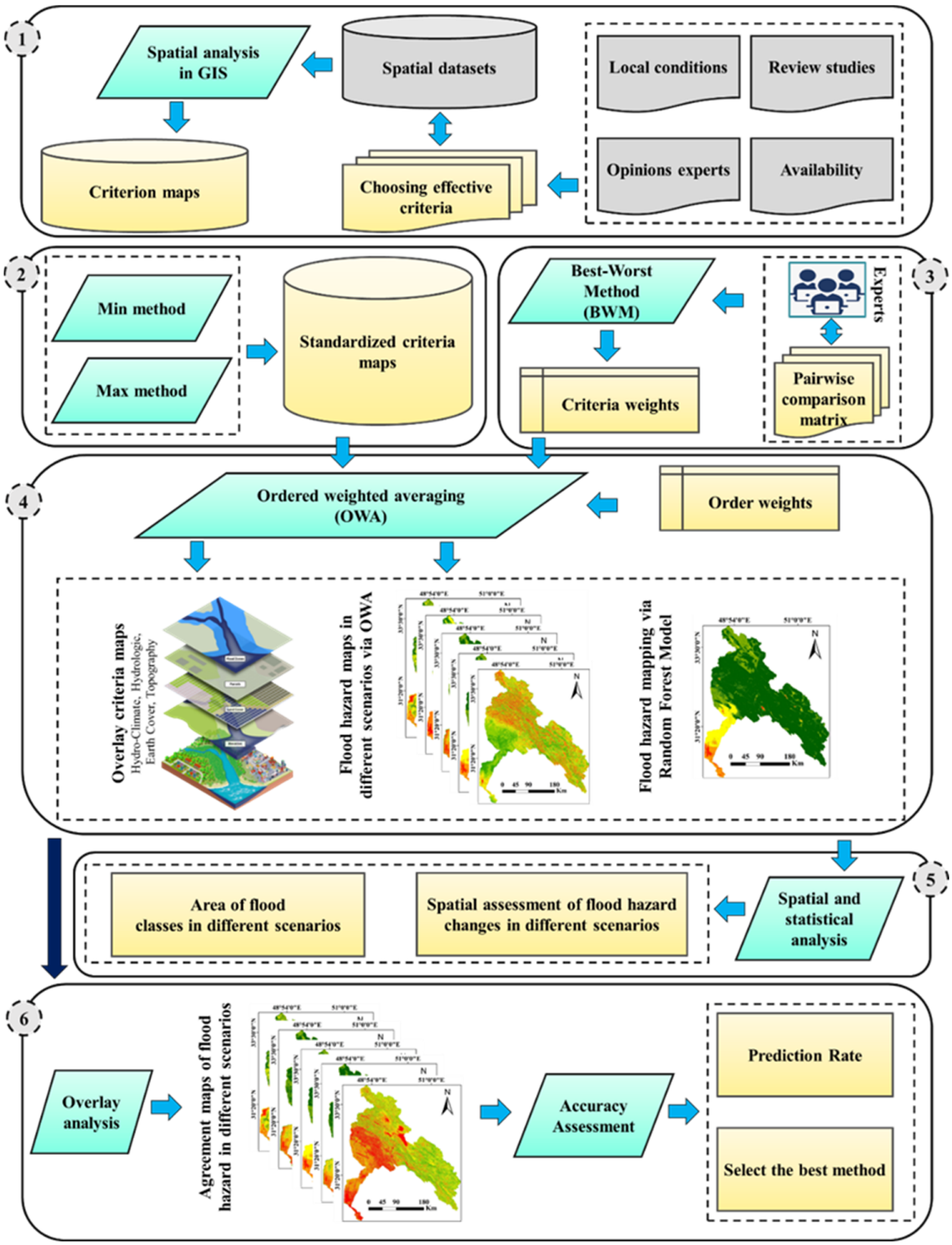


Figure 4. Flowchart of the current research methodology based on the different steps.

2.5. Best-Worst Method (BWM)

In the current study, the Best–Worst Method (BWM) was employed to determine the weights of the influencing criteria. This method, originally introduced by [46,47], was

considered one of the most efficient multi-criteria decision-making approaches, significantly enhancing the accuracy and consistency of judgments by reducing the number of required pairwise comparisons. Within the BWM framework, the decision-maker first identified the "best" and "worst" criteria based on their relative importance. Subsequently, the comparisons between the best criterion and all other criteria, as well as the comparisons between all criteria and the worst criterion, were conducted. This structured procedure ensured that the decision-maker's preference system was captured clearly and used as the analytical foundation for subsequent calculations. To derive the final weights of the criteria, a linear optimization model was then solved, with the objective of minimizing inconsistency in the provided judgments. The outcome was a set of weights that not only demonstrated the highest possible level of consistency but also provided an accurate representation of the decision-maker's preferences. Features such as reduced reliance on subjective assessments, high interpretability, robustness of results, and strong performance in complex evaluation settings make BWM a scientifically sound and reliable method for assessing and weighting flood-related criteria in this research. These advantages are particularly important in studies dealing with uncertainty and diverse environmental indicators, as they substantially enhance the precision and credibility of the final analysis.

In this study, expert judgments were collected from a panel of 20 academic experts and experienced practitioners with specialized knowledge in hydrology, water resources engineering, river engineering, remote sensing, and geomorphology. The experts were selected based on their academic background, publication records in reputable international journals, and their familiarity with the hydrological and environmental characteristics of the Great Karun watershed. To ensure the reliability of the Best-Worst Method (BWM) pairwise comparisons, the consistency of expert judgments was evaluated using the standard consistency ratio (CR) approach. The calculated CR values were found to be less than 0.10, indicating an acceptable level of consistency and logical coherence among expert judgments. Therefore, all expert opinions were considered reliable and were used in the final weight derivation process for the OWA-based flood susceptibility modeling.

2.6. Ordered Weighted Averaging (OWA)

The Ordered Weighted Averaging (OWA) operator was originally proposed by [48] as a flexible aggregation technique that provides a parametric framework for combining multiple criteria under different decision-making strategies. It was introduced as a flexible parametric aggregation framework for combining multiple criteria. For a given set of n criteria, the OWA operator is defined as a function $F : I^n \rightarrow I$, which is accompanied by a set of ordered weights in the form of $V = [v_1, v_2, \ldots, v_n]$. such that $V_j \in [0,1]$ for $j = 1,\ 2,\ \ldots,\ n$ and $\sum_{j=1}^{n} v_j = 1$. Now, if a set of standardized values for the criteria is available as: $A_i = [a_1, a_2, \ldots, a_n]$ for $i = 1, 2, \ldots, m$, where $a_{ij} \in [0,1]$ represents the value of the j-th criterion at the i-th position, then the OWA operator is defined as follows:

$$a \geq 0$$

$$OWA_i(a_{i1}, a_{i2}, \ldots, a_{in)} = \sum_{j=1}^{n} V_j Z_{ij} \quad (1)$$

Before implementing the OWA-based GIS-MCDA framework, all evaluation criteria must be expressed on a common measurement scale to ensure meaningful comparison and aggregation. Since the selected criteria differ in their units and value ranges, a standardization step was performed prior to the analysis. In this study, each criterion was normalized using its corresponding minimum and maximum values, thereby transforming the original data into dimensionless and comparable scores. Depending on the relationship between a criterion and flood susceptibility, two normalization strategies were adopted. Criteria with

a positive influence, where larger values indicate greater susceptibility, were treated as benefit criteria, whereas variables with an inverse relationship were considered cost criteria. Accordingly, Equations (2) and (3) were used to standardize the benefit- and cost-type criteria, respectively, before the OWA analysis. If a higher value is better (Maximize):

$$a_{ij} = \frac{S_{ij} - S_j^{min}}{S_j^{max} - S_j^{min}} \quad (2)$$

If a lower value is better (Minimize):

$$a_{ij} = \frac{S_j^{max} - S_{ij}}{S_j^{max} - S_j^{min}} \quad (3)$$

The OWA operator in Equation (1) focuses solely on the order weights, overlooking the fact that in many GIS-based spatial decision-making problems, it is necessary to define a separate weight for each criterion. To address this limitation, Ref. [49] proposed a method where attribute weights can also be incorporated into the calculation of order weights. This is achieved by modifying the structure of the OWA operator, with the goal of generating order weights that consider both the order of importance of criterion values and the overall importance of each criterion. In this approach, the main criterion weights are first incorporated into the calculation process, and then, using a specific formula (Equation (4)), the final order weights are obtained in proportion to the spatial location and the decision-making risk level.

$$V_j = \left(\frac{\sum_{l=1}^{j} u_1}{\sum_{l=1}^{n} u_1}\right)^{\alpha} - \left(\frac{\sum_{l=1}^{j-1} u_1}{\sum_{l=1}^{n} u_1}\right)^{\alpha} \quad (4)$$

In this method, u_j refers to the ordered weight of the j criterion, which is derived from its initial weight w_j based on the sorted values of the criteria Z_{ij}. The weight w_j for each criterion is determined by the decision-maker and indicates the relative importance of that criterion. These weights reflect the values and preferences of the decision-maker and have a constant value for the j criterion across all spatial locations. In contrast, the ordered weights u_j are calculated specifically for each spatial location (i) and are assigned to the sorted values of the criteria at that location, regardless of which criterion that value belongs to.

In other words, the highest criterion value at a location receives weight u_1, the second highest receives weight u_2, and so on. In GIS-based multi-criteria evaluations, criterion weights are usually defined such that their sum equals 1: $\sum_{j=1}^{n} w_j = 1$. Similarly, since u_j is just the sorted version of the same weights, their sum will also be equal to 1: $\sum_{j=1}^{n} u_j = 1$. Therefore, Equation (5) can be written as follows:

$$V_j = \left(\sum_{l=1}^{j} u_1\right)^{\alpha} - \left(\sum_{l=1}^{j-1} u_1\right)^{\alpha} \quad (5)$$

Given a set of criterion weights w_j and ordered weights v_j, the OWA operator can be defined as follows:

$$OWA_i = \sum_{j=1}^{n} \left(\left(\sum_{l=1}^{j} u_1\right)^{\alpha} - \left(\sum_{l=1}^{j-1} u_1\right)^{\alpha}\right) Z_{ij} \quad (6)$$

The value of α is related to the degree of ORness (or risk-taking propensity) [50]. The ORness value ranges from 0 to 1. This value indicates how much an OWA operator's aggregation behavior resembles that of a logical OR operator.

$$ORness = \frac{1}{\alpha + 1} \quad a \geq 0 \quad (7)$$

2.7. Machine Learning Model

Random Forest: The RF model is one of the advanced and widely used models in the field of supervised machine learning. By leveraging a collection of decision trees, it possesses a high capability in classifying and predicting complex and non-linear data. This model, by creating a number of independent decision trees through random sampling of data and features, and then aggregating their results as an average or majority vote, provides stable, accurate, and overfitting-resistant performance [51]. In the field of flood susceptibility mapping, the RF, by integrating spatial, hydrological, and climatic data, is capable of discovering hidden patterns in the relationships among variables and generating high-accuracy spatial susceptibility maps [52]. These characteristics have transformed the RF into an efficient tool for risk management, regional planning, and mitigating flood-induced damage.

From a computational perspective, RF operates based on the ensemble learning principle, where the final prediction is obtained from the collective behavior of multiple decision trees rather than a single classifier. During the training process, bootstrap sampling and random feature selection are applied to generate diverse tree structures, which improve model stability and reduce sensitivity to noise and overfitting. This mechanism is particularly advantageous for flood susceptibility assessment because environmental datasets often involve complex interactions, multicollinearity, and nonlinear relationships among conditioning factors. Furthermore, RF can estimate the contribution of individual predictors by analyzing the reduction in impurity produced by each variable during the tree construction process. Therefore, the model provides not only accurate classification of flood-prone areas but also a better understanding of the relative influence of hydro-environmental drivers controlling flood occurrence.

In this study, the RF model was optimized through careful tuning of key hyperparameters. The number of decision trees (n_estimators) was set to 250 to ensure a strong and stable ensemble performance. The maximum depth of each tree (max_depth) was restricted to 10 to control model complexity and reduce the risk of overfitting. In addition, the minimum number of samples required at each leaf node (min_samples_leaf) was set to 2 to maintain an appropriate balance between model generalization and spatial detail preservation.

To ensure a reliable model development and evaluation process, the dataset was divided into training and testing subsets using a random partitioning strategy, where 70% of the samples were allocated for model training, and 30% were reserved for independent testing and performance evaluation. The hyperparameters of the RF model were optimized using the Info-Optimizer algorithm [53] to determine the most suitable model configuration and improve predictive performance. The optimization process aimed to identify the optimal combination of RF parameters by minimizing prediction errors and enhancing the model's ability to generalize beyond the training data. The final RF structure was selected based on the optimized hyperparameter values, including the number of trees, maximum tree depth, and minimum samples required at leaf nodes. This approach reduced the risk of overfitting and provided a more robust framework for flood susceptibility prediction.

It should be noted that all computations and modeling procedures were performed using Python (3.10.8) in the Google Colab environment.

2.8. Model Performance Assessment

After generating flood susceptibility maps based on the outputs of different models, the study area was classified into five flood susceptibility classes: very low susceptibility (0–0.2), low susceptibility (0.2–0.4), moderate susceptibility (0.4–0.6), high susceptibility (0.6–0.8), and very high susceptibility (0.8–1.0). Model performance was evaluated using a

spatial validation approach based on the confusion matrix framework. First, the spatial extent of each susceptibility class was calculated as a proportion of the total study area. Then, observed flood locations (validation data) were overlaid on the susceptibility map to derive a confusion matrix, from which standard accuracy metrics were computed. For each class, Producer's Accuracy (PA) was defined [54] as:

$$PA_i = \frac{TP_i}{TP_i + FN_i} \tag{8}$$

where

- TP_i: number (or area) of correctly classified flood pixels within class iii
- FN_i: number (or area) of observed flood pixels that were not classified in class iii

The area proportion of each class was calculated as:

$$A_i = \frac{Area_i}{Area_{total}} \tag{9}$$

To further evaluate the ability of the model to concentrate flood occurrences in higher susceptibility zones, a Prediction Rate (PR) was defined as:

$$PR_i = \frac{PA_i}{A_i} \tag{10}$$

A higher Prediction Rate in high and very high susceptibility classes indicates a better capability of the model to correctly identify flood-prone areas relative to their spatial extent.

In classification tasks, Random Forest (RF) model predictions can be categorized into four possible outcomes: true positive (TP), true negative (TN), false positive (FP), and false negative (FN). In imbalanced datasets, where the number of samples belonging to one class is considerably higher than the other classes, conventional performance metrics may provide misleading interpretations of model effectiveness. Therefore, the Area Under the Receiver Operating Characteristic Curve (AUC-ROC) was employed as a reliable evaluation metric to assess the discrimination capability of the RF model.

The AUC quantifies the ability of the model to distinguish between positive and negative classes by evaluating the trade-off between the true positive rate (sensitivity) and false positive rate across different classification thresholds. Unlike accuracy-based metrics, AUC is less sensitive to class imbalance and provides a more comprehensive assessment of model performance. The AUC value ranges from 0 to 1, where values closer to 1 indicate excellent predictive capability, while values around 0.5 suggest that the model performs no better than random classification. In this study, the ROC curve was generated using the predicted probabilities of the RF model and observed flood occurrence data, and the AUC value was calculated using the trapezoidal integration method implemented in the Scikit-learn library.

Additionally, in this study, the Global Flood Database (GFD) dataset was carefully evaluated and compared with local observational data to ensure that the generated flood susceptibility maps were consistent with observed flood events, thereby enhancing the scientific validity and reliability of the results.

3. Results

A precise analysis of the indicators and variables influencing its occurrence and spread is of particular importance in understanding flood behavior at local and regional scales. To this end, in the current research, to provide accurate inputs for decision-making and machine learning models, a set of criterion maps was generated based on elevation

data and its derivatives, climatic data, and hydrological indicators. These maps are a reflection of the spatial complexities of the basin, and their interpretation can provide valuable information regarding flow paths, areas prone to inundation, and critical zones from a flood susceptibility perspective. Figure 3 displays four geographical maps, each representing a category of factors influencing flood occurrence in a specific watershed. These factors are divided into four main groups: hydro-climatic, hydrological, topographic, and land cover. Each map utilizes a color spectrum (primarily from green to red) to show the spatial variations in each criterion and, with the aid of a spatial scale and north orientation, provides a more precise data analysis capability. This type of multi-criteria classification is considered an efficient method for analyzing flood vulnerability at the basin scale.

Figure 5a, representing hydro-climatic factors, displays variables such as precipitation, temperature, evapotranspiration, and snow cover. Red areas indicate high levels of these variables, which can signify intense rainfall or a high runoff generation potential. These factors are particularly prominent in the northern and central highlands of the region, suggesting that these areas are more susceptible to flooding due to heavy and concentrated precipitation. Hydro-climatic analysis is considered the first step in understanding the potential of rainfall leading to floods.

Figure 5b pertains to hydrological criteria, which include factors such as drainage density, distance from the river, distance from dams, the river stress index, and cumulative flow. The pattern observed in this map exhibits a relatively more homogeneous texture compared to the first map; however, areas with reddish tones are still visible in certain parts of the downstream basin, which may indicate reduced infiltration capacity or increased surface runoff. This analysis helps determine how and at what rate rainfall flows and accumulates across the basin.

Figure 5c relates to land cover and has been produced considering criteria such as surface cover, soil class, geological class, and vegetation cover. In this map, the influence of various surface cover types such as forests, rangelands, agricultural lands, and built-up areas on the hydrological behavior of the basin is examined. Areas shown in red indicate poor cover or land uses with low permeability and high runoff generation (such as urban areas or compacted agricultural lands). In contrast, green areas typically have dense vegetation that effectively reduces runoff. Land cover analysis is essential for assessing land-use changes and managing land use to reduce flood risks.

Figure 5d represents the topographic characteristics of the watershed, including slope, elevation, the topographic wetness index, curvature, and the river sediment transport index. Areas shown in red generally indicate steep slopes or high elevations, which have a greater potential for rapid runoff concentration and the formation of flood flows. Topography not only influences the direction and velocity of water flow but also plays a key role in identifying areas prone to erosion, landslides, and surface runoff concentration. Therefore, precise analysis of topographic indices is essential for designing flood-warning systems and runoff-control structures.

The combination of four categories of flood-influencing factors, including hydro-climatic, hydrological, topographic, and land-cover criteria and indices, provides a systematic, coherent, and multidimensional framework for spatial analysis of flood susceptibility. Since flooding is a complex phenomenon resulting from the interaction of natural and human factors across variable spatial and temporal scales, the simultaneous use of these four groups of information enables a more comprehensive assessment of flood dynamics at the watershed level. These factors not only affect the hydrological behavior of the basin independently, but their spatial combination can also identify flood-prone areas with higher accuracy.

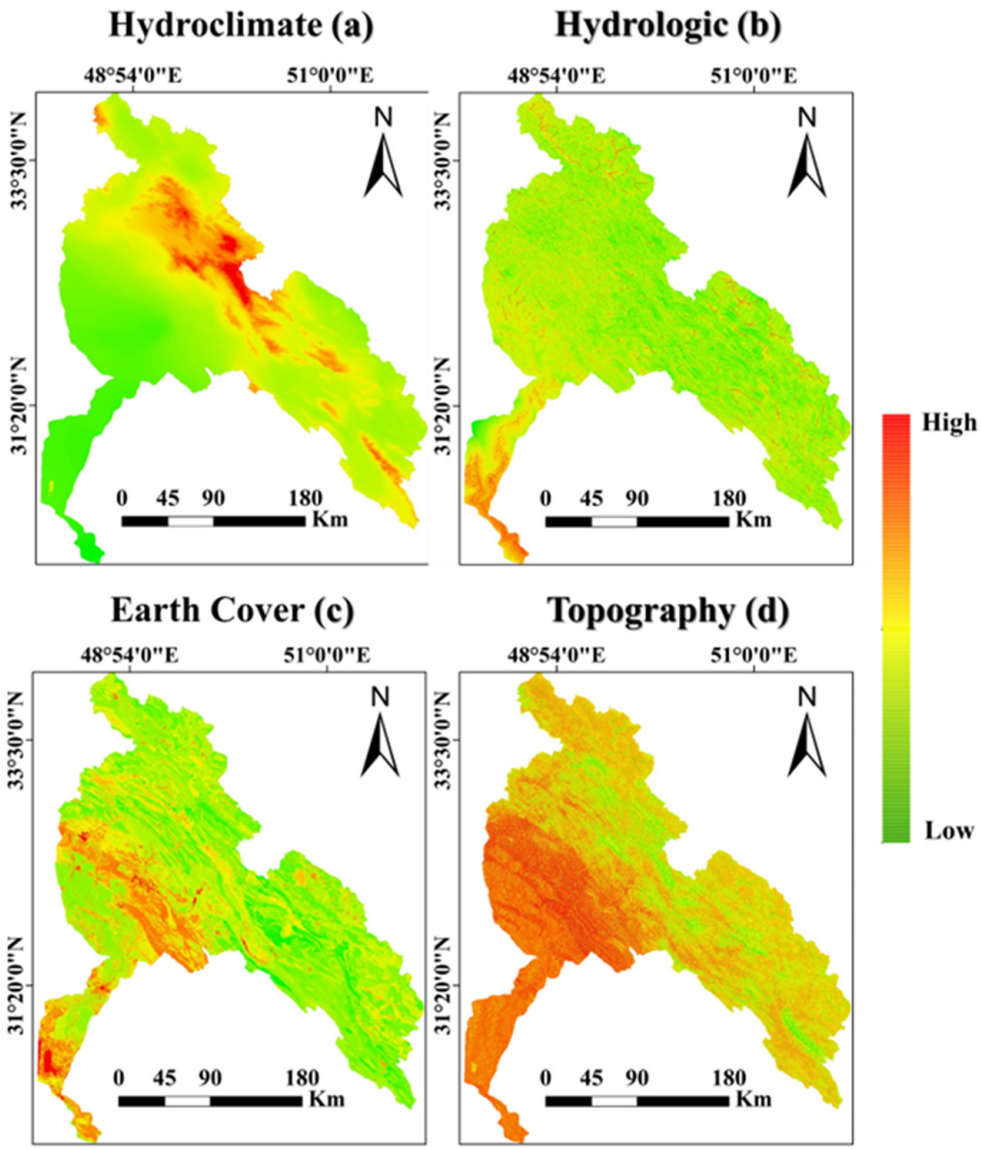


Figure 5. Criteria Integrating Flood susceptibility; Hydro-Climate (**a**), Hydrologic (**b**), Earth Cover (**c**), and Topography (**d**).

In terms of hydrological analysis, understanding flood behavior in different parts of the watershed, including upstream, midstream, and downstream, has particular importance. Upstream areas typically have steep slopes, high rainfall, and natural vegetation cover, which, although they generate rapid runoff, can also exhibit high storage and infiltration capacity. In contrast, midstream areas often act as pathways for surface flows and, as transitional zones, are more affected by the combined conditions of upstream regions and their own land-use characteristics. The downstream part of the basin, which usually includes low-slope plains with concentrated settlements and agricultural lands, has the highest vulnerability to runoff accumulation and overflow; according to land-cover and hydrological maps, these areas generally have low permeability, dense structural development, and short distances to waterways, which intensify flood risk. Continuing this analytical approach, the present study will examine flood-susceptibility mapping under five probable scenarios that range from highly optimistic to highly pessimistic. These scenarios represent a spectrum of environmental and managerial conditions that may occur in the future of the basin. In the optimistic scenarios, relatively stable and favorable conditions are assumed for the watershed, while in the moderate and pessimistic scenarios, the intensity

of threatening factors gradually increases and potential hazards rise. In each scenario, the spatial pattern of flood susceptibility in the upstream, midstream, and downstream sections will be analyzed to reveal differences in watershed behavior under varying conditions. This scenario-based analysis provides a foundation for better understanding possible futures and making informed decisions in flood-risk management.

Figure 6 shows the results of flood susceptibility zoning based on using the RF model and OWA operator with the ORness index across five different scenarios (0 = completely pessimistic, 25 = pessimistic, 50 = realistic, 75 = optimistic, and 100 = completely optimistic). Each scenario represents decision-making behavior with varying degrees of risk aversion, from completely pessimistic to completely optimistic. Analysis of the maps indicates that as the ORness value decreases, the data combination becomes more conservative, emphasizing the worst possible conditions. Consequently, in the completely pessimistic scenario (ORness = 0), a wide area of the region, particularly the south and southwest, falls into the high to very high-risk categories. The reason could be the influence of parameters such as low slope, proximity to rivers, and impermeable soil textures. This magnification is intentionally implemented to cover all high-risk areas and to reduce the risk of the analysis.

As ORness increases towards the mid and higher values (25, 50, and 75), the extent and distribution of high-risk areas decrease, and the risk becomes confined to more specific and realistic areas such as main river paths and low-lying regions. The ORness = 50 scenario, which represents a balanced behavior between optimism and pessimism, offers a realistic view of the risk status and is considered the reference scenario for subsequent analyses. In the completely optimistic scenario (ORness = 100), most of the area is categorized as low-risk, with only limited areas exhibiting specific geographical features, such as proximity to main rivers, remaining in the medium to high-risk classes. Comparing these scenarios with the results of the RF machine learning model shows that RF also identifies the southern parts of the basin and the floodplains as areas with persistent high risk, which highlights a relative consistency with the results of the intermediate and pessimistic OWA scenarios. However, unlike the pessimistic scenarios that encompass a wide range of areas, the RF model identifies the risk in a more concentrated and targeted manner, avoiding overestimation of high-risk areas. Furthermore, compared to the completely optimistic scenario, the RF model tends to predict a higher and more conservative risk, which is due to the model's ability to utilize actual data and assign weights to influential variables. The spatial sensitivity analysis and the overlap matrix between the RF results and the OWA scenarios indicate that the highest spatial correspondence is related to the ORness = 50 scenario, where approximately 70% of the high-risk areas are common in both models, while the completely optimistic scenario has only about 30% overlap. This suggests that ORness = 50 is a suitable representative for a realistic and balanced analysis that can serve as a basis for decision-making in flood risk management planning. Another important point is the persistence of high-risk areas across all scenarios and the RF model; specifically, the southern sections and floodplains, which are exposed to medium to high risk even under the most optimistic conditions. This spatial risk persistence underscores the necessity of focusing and prioritizing engineering measures such as the construction of flood control structures, improvement of drainage systems, and land-use management in these areas.

In summary, the combination of scenario-based analysis using the OWA model with the data-driven output of the RF model provides a comprehensive perspective on the extent and distribution of flood risk and the impact of different decision-making behaviors when faced with uncertainty. This multi-scenario approach allows for flexible planning and resource optimization for flood risk management in the region. In other words, compared to classical models, this approach offers greater flexibility in responding to

uncertain conditions and can play a significant role as a decision support tool in managing natural hazards.

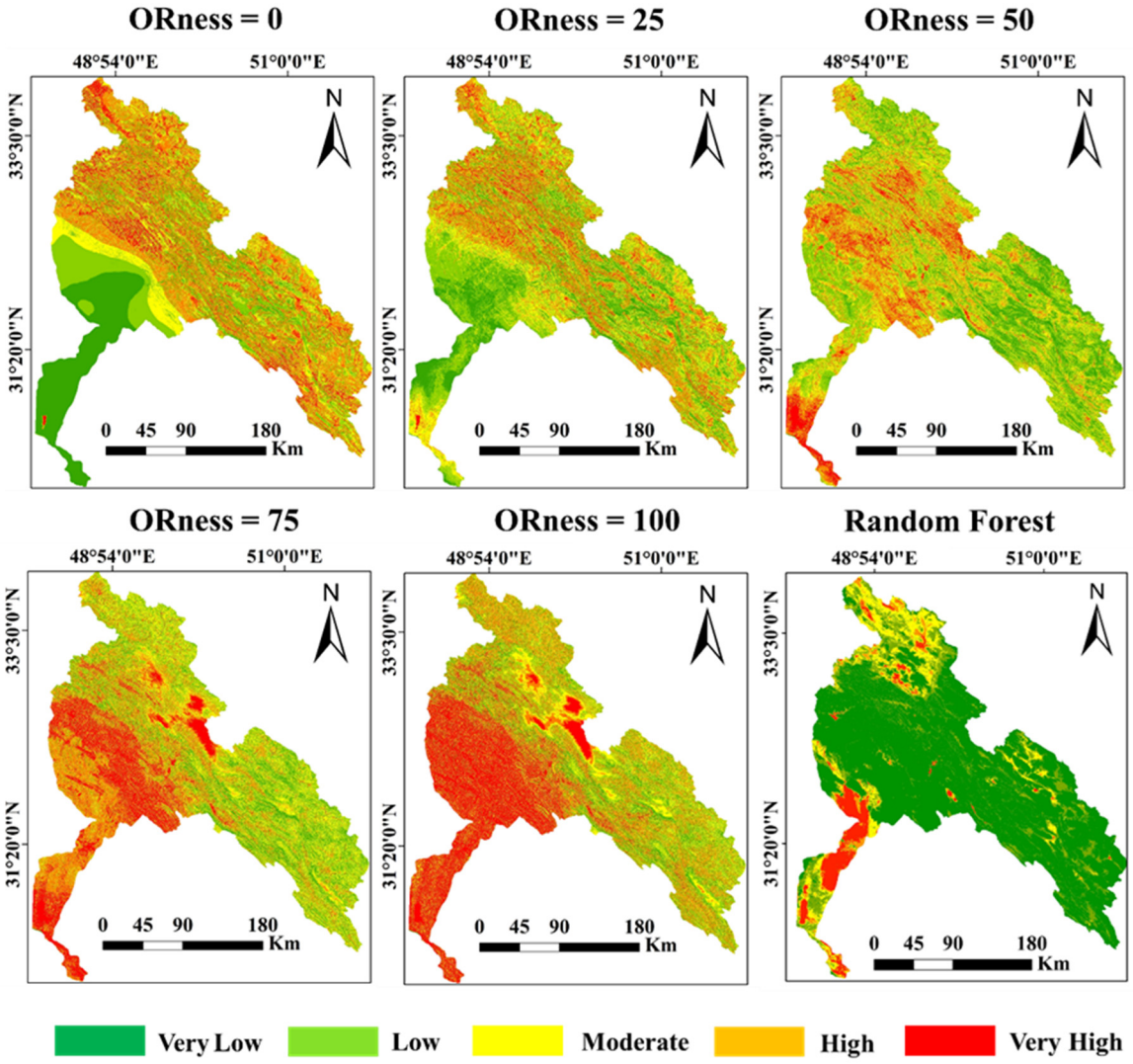


Figure 6. Flood susceptibility prospectively maps for the selected values of ORness and RF model.

3.1. Comparative Analysis of RF Model Performance and OWA Scenarios with Different ORness Levels Based on Prediction Rate Index

According to the OWA model in the completely pessimistic scenario (ORness = 0), where all weights are assigned to the lowest values, the highest prediction rate is observed in the "Very Low" class (2.8%). As the risk class increases, the prediction rate continuously decreases, reaching 0.3% and 0.6% in the "Medium" and "High" classes, respectively, and only 1.4% in the "Very High" class. This indicates that this scenario is more effective in identifying low-risk areas but performs poorly in detecting high-risk areas. With a slight increase in ORness in the pessimistic scenario (ORness = 25), a noticeable change in the prediction rate is seen in the higher classes, with the "Very High" rate increasing from 1.4% to 2.2%. Consequently, while maintaining accuracy in the lower tiers, areas with a high probability of flooding are better identified, and performance in the "Low" and "Medium" classes is more balanced. This scenario is significant from the perspective of balancing conservatism and realism.

In the logical or neutral scenario (ORness = 50), weights are distributed evenly, and a clear increase in the prediction rate for higher probability classes is observed. The rate for the "Very High" class reaches 3.5%, the highest value among the scenarios. This

scenario provides a balance point between risk coverage and reducing decision-making risk, as the increase in rates in the higher classes does not come with a sharp decline in the lower classes. In the optimistic scenario (ORness = 75), the tendency to focus on higher criterion values increases, and the prediction rate in the "High" class reaches 1.8%. However, in the "Very High" class, it is only 1.9%, which is lower than the corresponding value in the neutral scenario. The sharp decrease in rates for the "Very Low" and "Low" classes (0.2% and 0.4%, respectively) indicates that the model has lower discriminative power in the initial tiers and primarily focuses on higher-risk areas, although not with sufficient accuracy.

In the completely optimistic scenario (ORness = 100), the highest prediction rate in the "Very High" class is 2.2%, which is lower than the corresponding value in the neutral scenario (3.5%). This suggests that increasing ORness does not necessarily guarantee improved identification of high-risk areas. Furthermore, the rates for the "Very Low" and "Low" classes decrease to the lowest possible level (0.2%). Overall, this scenario carries a high risk in decision-making as its focus is on ranges that may not align with actual risks.

3.2. Analysis of Random Forest Model Performance Compared to OWA Scenarios

The RF machine learning model (Figure 7) demonstrates remarkable performance across all classes, especially in the upper-risk tiers. The prediction rate in the "Very High" class reaches 16.02%, a figure that is not only significantly higher than all OWA scenarios but also indicates the model's strong ability to understand the relationships and complexities among criteria, as well as its precise focus on high-risk areas with minimal spatial waste. Furthermore, the prediction rates in the "High" (7.56%) and "Medium" (4.67%) classes are also at a high level, signifying the model's balance and high accuracy in differentiating sensitive areas. Conversely, in the "Very Low" and "Low" classes, the prediction rate is very low (0.09% and 0.68%, respectively), suggesting that the model does not tend to predict low-risk areas as critical. This is a desirable characteristic in risk and disaster management, as it reduces false alarms and enhances decision-making accuracy during crisis management.

Therefore, the results indicate that as ORness increases in the OWA method, the model moves towards greater optimism in selecting critical areas, but this optimism is consistently associated with a decrease in the actual prediction rate in the upper tiers. In contrast, the RF model, relying on data-driven learning power and non-linearity, has identified the spatial distribution of flood risk with significantly higher accuracy than the OWA method. Consequently, if the objective is to focus on accurately predicting high-risk flood areas with the least occupied area, RF is recognized as the best option in terms of prediction performance. However, if the decision-making approach is based on subjective preferences and uncertainty assessment strategies, the OWA scenario with ORness = 50 (logical) provides the greatest balance between conservatism and prediction accuracy. Figure 5 displays the values and comparisons based on the prediction rate.

The RF model in flood susceptibility zoning demonstrates a remarkable and superior performance compared to the OWA-based scenarios and method, achieving an AUC criterion of 0.984 (Figure 8). This high AUC accuracy suggests the high capability of the RF model in correctly distinguishing areas with high flood risk from low-risk areas. In comparison, the OWA method, which includes a degree of subjective judgment in weighting the factors affecting floods, could not achieve the same level of accuracy and reliability as the RF model in identifying and classifying high-risk areas. Therefore, the RF model, as a data-driven method, highlights a more powerful tool for accurate flood risk assessment and zoning in this study.

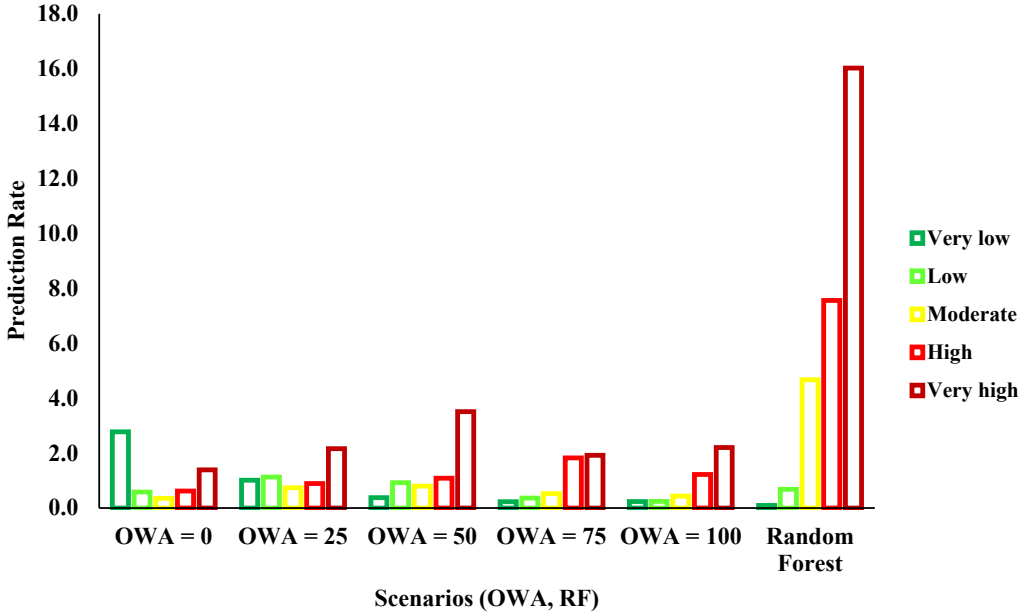


Figure 7. Prediction Rate (PR) for different flood probability classes.

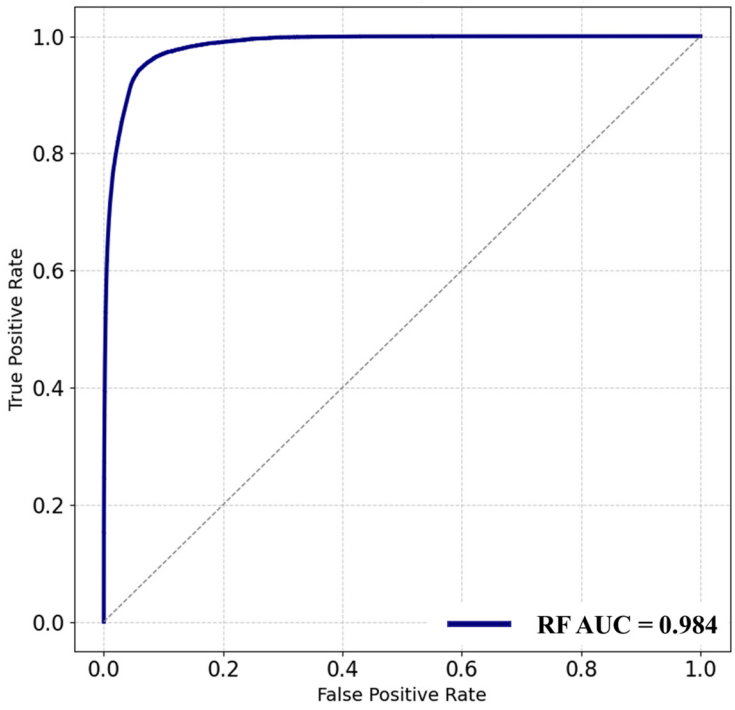


Figure 8. AUC Curve of RF model.

To assess whether the observed differences in model performance are statistically significant, a non-parametric Wilcoxon signed-rank test was conducted at a 95% confidence level ($\alpha = 0.05$). The test was applied to the spatial prediction results of the Random Forest (RF) and OWA-based models using the same independent validation dataset. The results indicate that the difference between the RF model and all OWA scenarios is statistically significant ($p < 0.05$), confirming that the superior performance of the RF model is not due to random variation. In addition, bootstrap resampling (1000 iterations) further supported the robustness of these findings, showing consistently higher AUC values for the RF model across repeated samples.

3.3. Quantitative and Comparative Analysis of Flood Risk Classes Based on OWA and RF Models

Figure 9 reveals the percentage of the study area belonging to each of the five flood probability classes, from very low to very high, for different scenarios of the OWA model and the RF model. This distribution of classes illustrates how each model or scenario responds to data and uncertainty in determining flood risk levels on a spatial scale. By analyzing this data closely, one can evaluate the behavioral and performance differences in each scenario and model. Based on the OWA model in the completely pessimistic scenario (ORness = 0), nearly half of the area (49.6%) falls into the "Very Low" class, which is the largest proportion among all scenarios. This outcome stems from the complete focus on the minimum values in the decision-making criteria, such that any area where at least one characteristic is within the safe range is generally classified as low-risk. Consequently, the northern and northeastern parts of the basin—with moderate to high slopes and permeable soils—are placed in the lower risk classes, while the low-lying plains of the southwest and areas adjacent to rivers remain in the "High" and "Very High" classes, indicating the strong effect of dominant features such as low elevation and poor drainage. With a slight increase in ORness in the pessimistic scenario (ORness = 25), the proportion of the "Very Low" class decreases to 18.2%, and the "Low" class increases to 33.5%, leading to a more balanced risk distribution. In this case, areas with a combination of opposing characteristics, such as high slope but close proximity to the river, are placed in the "Medium" or higher classes, and parts of the central and western basin appear to be at greater risk, signifying the model's transition from extreme conservatism to a more balanced assessment.

The logical or neutral scenario (ORness = 50) shows the most balanced distribution, with the largest area proportion in the "Medium" class (22.9%). Approximately 43.1% of the area is located in the "High" and "Very High" classes, primarily comprising downstream plains, areas near major networks, and impermeable soils. This combination indicates that the model, without exaggeration, identifies areas of high cumulative risk while keeping areas with mixed conditions at a medium level, which is suitable for optimal resource allocation and resilient infrastructure design. In the optimistic scenario (ORness = 75), approximately 76% of the area falls into the "High" (46.4%) and "Very High" (29.2%) classes, reflecting the strong influence of parameters with high values. Even the presence of a single critical variable moves a cell into the high-risk category. Areas such as the southern plains, the edges of major rivers, and regions with impermeable soil and low slopes are more prominent than before. This scenario is applicable to emergency situations and resilience analysis of infrastructure. In the completely optimistic scenario (ORness = 100), over half of the area (52.4%) is classified as "Very High" because the model exclusively weights the maximum values, classifying areas with one critical criterion as high-risk zones regardless of other safe characteristics. Large parts of the southern and southeastern basin, even areas with resilient features, are placed in the high class. This indicates that although this scenario is theoretically optimistic, in practice, it can exaggerate potential risks and requires careful interpretation and use.

The comparative assessment of the RF model with different OWA scenarios reveals significant differences in how flood risk is evaluated and spatially distributed. Based on the results, the largest area proportion in the RF model corresponds to the "Medium" risk class (35.5%), indicating the model's tendency to identify areas with a mid-level, realistic risk. This characteristic contrasts with some OWA scenarios, such as ORness = 0 or ORness = 100, which have resulted in heavily conservative or optimistic distributions, respectively. In terms of high-risk classes (the sum of "High" and "Very High" classes), the RF model, with a share of 47.85%, shows a relative similarity to the ORness = 50 and ORness = 75 scenarios. However, its distribution is far more structured and lacks exaggeration in identifying high-risk areas. In OWA scenarios with lower ORness values (such as 0 and 25), the

proportion of high-risk classes is lower, and the model tends towards underestimating the risk. Conversely, in high ORness scenarios, particularly ORness = 100, a very large portion of the area (over 80%) falls into the "High" and "Very High" classes, indicating a potential overestimation of risk and high sensitivity to extreme values of spatial parameters.

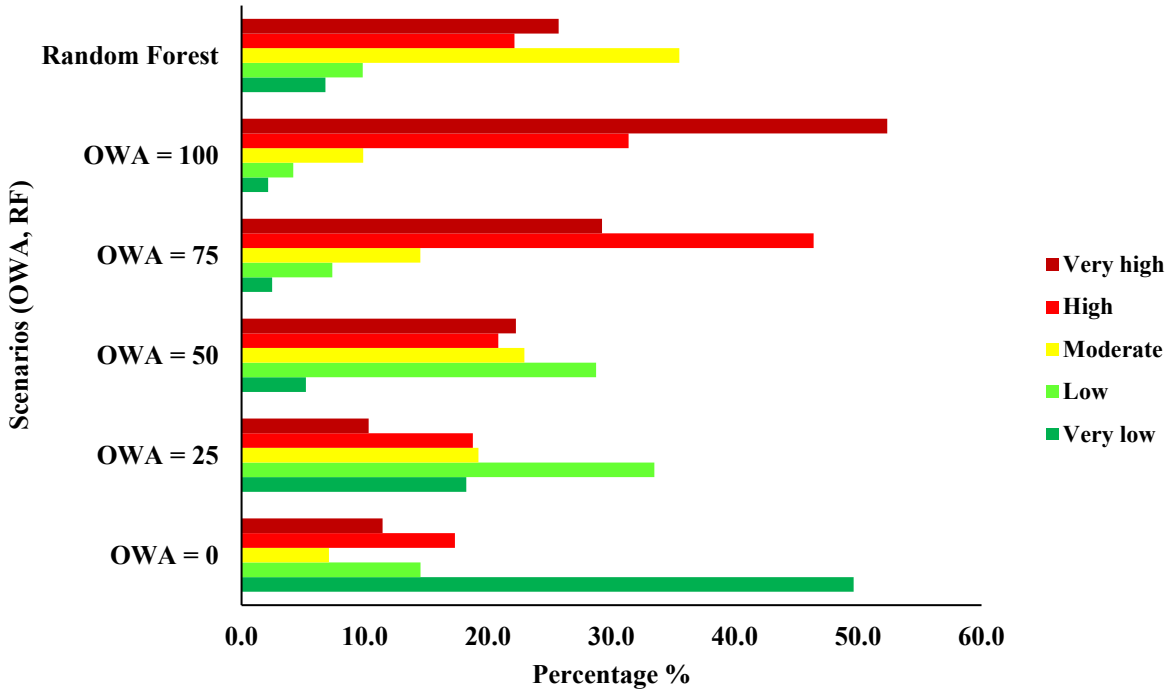


Figure 9. Percentage of the study area assigned to each flood probability class—Class area (%).

Overall, the results suggest that the ORness = 50 scenario of the OWA model exhibits the most statistical and conceptual alignment with the RF model. This scenario has managed to strike a balance between optimism and pessimism, providing a relatively balanced risk distribution across the area. Therefore, it can be considered a benchmark scenario in OWA-based analyses. In contrast, the RF model, with its data-driven performance and reliance on statistical experience, is a suitable option for situations where accurate historical information and reliable environmental data are available, and decision-making requires reality-based analyses devoid of subjective assumptions. In general, the comparison between these two approaches, OWA and RF, indicates that their combined use can provide a comprehensive and powerful approach to flood risk management. The OWA model, with its scenario-based analysis capability, is a suitable tool for analyzing uncertainty and evaluating decision sensitivity, while the RF model can offer accurate and operational predictions by identifying hidden patterns within the data. This analytical integration is particularly valuable for strategic decision-making in regional planning, resource management, and the design of flood-resilient structures.

Analysis of risk maps and the percentage distribution of their classes across different models is a key tool for understanding the variations in flood assessment at a regional level. In this study, the OWA approach was utilized with five distinct ORness levels, ranging from completely pessimistic to completely optimistic, alongside the RF model for comparative analysis and validation. The various OWA scenarios facilitate the examination of different decision-making strategies under uncertainty, while the RF model, with its data-driven approach, offers precise predictive capabilities based on trained data. The following presents a comprehensive analysis of flood risk class distribution within each of these scenarios. Figure 10 visually depicts the percentage distribution of actual flood occurrence locations across the different flood probability risk classes.

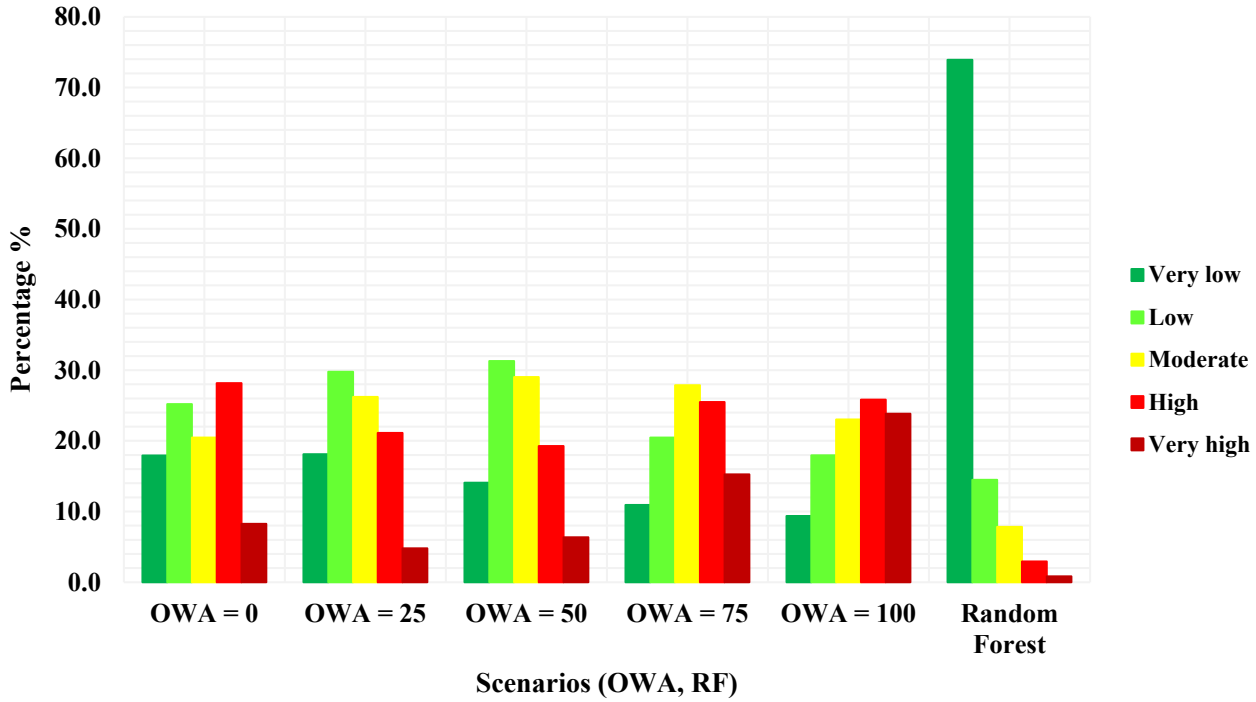


Figure 10. Percentages of actual flood occurrence locations within each flood probability class.

For the completely pessimistic scenario (ORness = 0), which indicates the highest degree of caution in decision-making, approximately 17.9% of the area falls into the "Very Low" risk class. This high percentage is due to the weighting being focused on the minimum input values of the criteria; therefore, even if only one of the influential criteria is in a safe condition, that area is considered low-risk. The northeastern parts of the basin, which have favorable elevation and permeability conditions, are mainly assigned to lower risk classes, while the southern and southwestern areas, with low-lying terrain and high surface runoff density, remain in the "High" and "Very High" classes. The pessimistic scenario (ORness = 25), with a slight increase in the "Very Low" class share to 18.1% and a relative growth in the "Low" class, indicates a decreased focus solely on minimum values and greater attention to intermediate values; such that areas with contradictory features, like steep slopes but proximity to a river, are placed in higher classes. This distribution signifies a transition from strict decision-making to a more balanced approach, and parts of the basin's center, previously in lower classes, are now seen in the middle tiers.

In the logical or neutral scenario (ORness = 50), the model reaches a balance between optimism and pessimism, and the class distribution appears more logical; the largest share of the area falls into the "Medium" class, and the combined share of "High" and "Very High" classes is approximately 25%. This scenario places areas with a combination of high-risk parameters into higher classes and keeps areas with mixed characteristics in the medium class, serving as a suitable reference scenario for realistic analyses. With increasing optimism in the optimistic scenario (ORness = 75), the impact of high criterion values increases, and the share of "High" and "Very High" classes reaches 40.7%; areas where even one of the risk factors is high are quickly placed in the higher risk classes, and the southern parts and areas around rivers have emerged with greater concentration as high-risk zones. This approach is applicable for designing emergency policies and protective planning, but there is also a possibility of overestimating the risk in balanced areas. In the completely optimistic scenario (ORness = 100), over 49.6% of the region falls into the "High" and "Very High" classes, as the weighting is solely focused on the highest value of each criterion; even the presence of a single critical criterion leads to the area being labeled as high-risk. This

scenario offers the broadest risk identification and is useful for maximalist analyses, but requires caution and precise interpretation in operational policymaking.

However, in the RF model, the largest share of the region's area falls into the "Very Low" class (73.9%), and the combined "High" and "Very High" risk classes cover only 3.7% of the total area. This distribution indicates that the RF model has a conservative approach, underestimating the risk probability for most areas. Unlike the OWA scenarios with high ORness that focus on high-risk classes, RF tends to underestimate flood occurrences. Nevertheless, its distribution's proximity to lower ORness scenarios, especially OWA = 0 or 25, suggests that this data-driven model, by focusing on historical patterns, exhibits a relatively conservative behavior in identifying high-risk areas.

Therefore, comparing the results from the OWA model across different scenarios with the RF model reveals significant differences in how flood risk is assessed and displayed at a regional scale. While the OWA scenarios allow for the analysis of sensitivity and uncertainty, the RF model possesses the capability to identify complex patterns within the data. The ORness = 50 scenario from the OWA model shows the greatest statistical and conceptual similarity to the RF model and can be considered the reference scenario for scenario-based analyses. In contrast, very low or very high ORness levels have led to underestimation or overestimation of risk, respectively. These analyses indicate that a combined approach utilizing judgment-based models like OWA and data-driven models like RF can provide a comprehensive, accurate, and practical approach for flood risk management in real and complex conditions. The simultaneous use of these models helps decision-makers benefit from both conservative viewpoints and empirical analyses, ultimately leading to the design of more efficient and sustainable policies and plans.

3.4. Validation of Flood Susceptibility Mapping via Observed Flooded Points

In this study, after generating the flood susceptibility maps, the resulting outputs were validated using 150 observed flood field points (2000-2019). The validation was carried out through a geospatial analysis approach in a GIS environment, employing spatial overlay techniques to assess the correspondence between predicted flood-prone areas and actual inundation locations. This method allowed for an accurate evaluation of spatial agreement between model outputs and observed flood events (Figure 11). This dataset was accurately documented with high spatial precision by the Khuzestan Water and Power Authority (www.kwpa.ir). This evaluation served as a criterion for measuring the performance, accuracy, and generalizability of the model used in identifying flood-prone areas [55]. Preliminary results indicated that the RF model employed has acceptable accuracy in reproducing flood spatial patterns and determining high-risk areas. The conducted analysis shows that the RF model, by classifying 73.5% of flood points in the "very high" class and a total of 87.7% in the "high" and "very high" classes, demonstrated the best performance. This high accuracy indicates that the RF model has a reliable capability in flood risk classification. This finding emphasizes that the RF model possesses high sensitivity and accuracy, particularly in the initial identification of high-risk areas, and its use for risk management and urban development planning is trustworthy. Furthermore, data from the GFD (Global Flood Database) also showed satisfactory accuracy and reliability for use in flood sensitivity modeling, risk assessment, and mapping. These datasets are powerful and perform well in representing the spatiotemporal patterns of flood frequency [56].

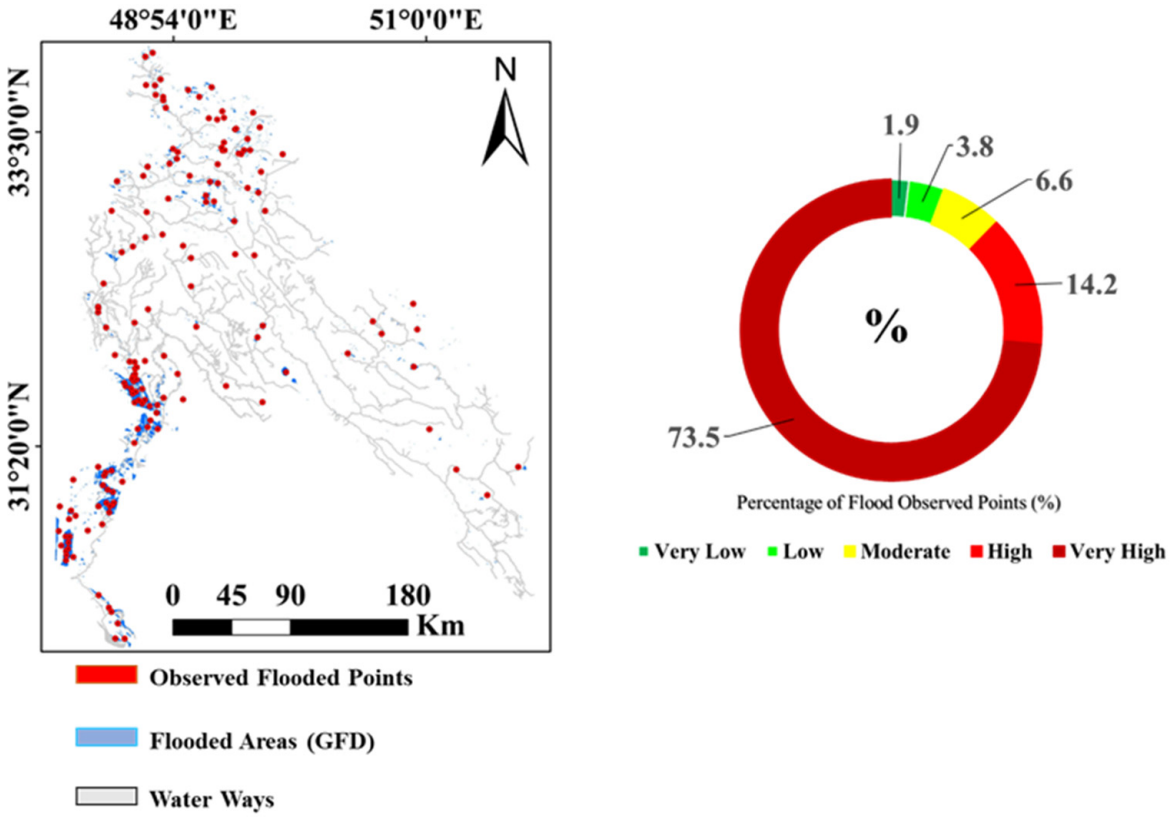


Figure 11. Assessment of field flood points distribution and their correspondence with flood susceptibility classes predicted RF.

4. Discussion

The findings of the current study highlight the potential of two fundamentally different approaches: a knowledge-driven multi-criteria decision-making framework based on expert judgment and scenario construction (OWA), and a data-driven machine learning model (Random Forest), which together provide a multi-layered perspective on flood risk behavior within the Great Karun basin. The pronounced differences in flood susceptibility patterns generated by these two approaches, particularly in areas characterized by complex hydrological conditions, indicate that the subjective nature of weighting in MCDM methods can increase the sensitivity and variability of the results. In contrast, data-driven models, by exploiting statistical structures and hidden nonlinear patterns in the data, produce more stable and realistic outcomes. This clearly suggests that reliance on a single methodological framework may provide an incomplete representation of the flood risk landscape.

The comparison of influential conditioning factors revealed a noticeable mismatch between expert-based judgment and data-driven evidence. In the OWA approach, variables such as distance from rivers and slope, which are traditionally considered geomorphologically significant, received the highest weights. Conversely, the RF model identified precipitation and flow accumulation as the most influential predictors of flood hazard, reflecting its ability to capture complex interdependencies among variables. This discrepancy demonstrates that subjective weighting schemes tend to emphasize more visible and intuitively interpretable factors, whereas machine learning approaches can uncover less apparent but highly influential drivers. This finding further highlights the importance of integrating data-driven methods to reduce cognitive and methodological biases in flood susceptibility assessment.

From a broader scientific perspective, these findings are consistent with a growing body of literature comparing multi-criteria decision-making (MCDM) approaches and

machine learning models in flood susceptibility mapping. Previous studies have generally reported that MCDM frameworks such as AHP, WLC, and OWA offer transparent and flexible decision-support structures; however, they are highly dependent on expert judgment and weighting schemes, which may introduce subjectivity and spatial variability in hazard zoning. In contrast, machine learning models, particularly Random Forest, have demonstrated superior capability in capturing nonlinear and high-dimensional relationships between flood conditioning factors, often leading to higher predictive accuracy and robustness. Nevertheless, several studies have also emphasized limitations of machine learning approaches, including reduced interpretability and sensitivity to data quality and representativeness. In this context, the present study not only confirms these general findings but also extends them by showing that model performance and dominant conditioning factors may vary under different hydro-climatic settings within the Great Karun basin, emphasizing the necessity of regional calibration and context-specific evaluation.

The analysis of optimistic to pessimistic scenarios within the OWA framework demonstrated that the degree of risk tolerance and subjective weighting structure directly influence flood risk estimation. Optimistic scenarios systematically tended to overestimate flood risk due to reduced sensitivity to worst-case conditions, whereas pessimistic scenarios tended to underestimate risk by emphasizing conservative aggregation behavior. The neutral scenario exhibited the highest statistical similarity with the RF model and can therefore be considered a balanced reference under moderate uncertainty conditions. This behavior indicates that scenario-based approaches, while flexible and interpretable, are highly dependent on the decision-maker's subjective assumptions and therefore require validation against data-driven approaches.

The Random Forest model demonstrated robust performance in flood risk classification, achieving an AUC value of 0.984 and accurately identifying highly vulnerable areas. Its ability to capture nonlinear relationships, model complex interactions among variables, and resist overfitting makes it a powerful tool for flood susceptibility assessment in highly complex hydrological environments. The clear superiority of RF over OWA suggests that data-driven approaches not only provide higher predictive accuracy but also greater stability under data variability. This performance highlights the strong applicability of machine learning models for early warning systems, land-use planning, and disaster risk management in flood-prone regions.

Overall, the results of this study have important implications for flood risk management. First, the integrated use of scenario-based MCDM approaches and data-driven machine learning models can provide a more comprehensive and multidimensional understanding of flood risk dynamics, compensating for the limitations of each individual method. Second, the application of data-driven models, particularly in heavily human-impacted watersheds, can support more realistic, robust, and evidence-based decision-making processes.

Beyond methodological insights, the outcomes of this study also have important implications for sustainable watershed management, climate adaptation, and disaster risk reduction strategies. Furthermore, the findings of this study contribute to several Sustainable Development Goals (SDGs) by supporting effective disaster risk reduction [57], sustainable watershed management, and climate-resilient planning. The proposed flood susceptibility mapping framework contributes to SDG 11 (Sustainable Cities and Communities) by improving the identification of flood-prone areas and enhancing the resilience of communities, infrastructure, and land-use planning against flood hazards. Moreover, the integration of hydro-climatic variables and advanced modeling approaches supports SDG 13 (Climate Action) by providing scientific evidence for climate adaptation strategies and risk-informed decision-making under changing environmental conditions [58]. The results

also align with SDG 6 (Clean Water and Sanitation) by improving the understanding of watershed hydrological responses and supporting sustainable water resources management policies [59], including flood control planning [60], integrated watershed management, and more efficient allocation of water-related resources. Therefore, the proposed RF-OWA framework can serve as a decision-support tool for water managers and policymakers to develop adaptive strategies for reducing flood impacts and improving the long-term sustainability of water systems.

Weighting of Layers and Extraction of Effective Criteria via BWM and MDI Algorithm

Table 2 lists the weighting of layers of effective flood criteria based on the Best-Worst method, which, due to the superior performance of the RF algorithm in flood risk zoning across different classes, derived the weights of the criteria in the modeling process based on the Mean Decrease in Impurity (MDI) algorithm.

Table 2. Weighting of Flood Influential Criteria and Feature Importance Based on the BWM Method and the MDI Algorithm, respectively.

Criteria	Expert-Assigned Weight	Sub-Criteria	Expert-Assigned Weight	RF-Feature Importance Via MDI
Hydro-Climate	0.37	Precipitation	0.47	0.66
		Temperature	0.17	0.52
		Evapotranspiration	0.1	0.58
		Snow Cover	0.26	0.18
Hydrologic	0.29	Distance To Streams	0.17	1.14
		Drainage Density	0.15	0.43
		Distance To Dams	0.12	0.68
		Stream Power Index (SPI)	0.23	0.29
		Flow Accumulation	0.33	0.75
Earth Cover	0.2	Vegetation Cover (NDVI)	0.33	0.91
		Land Cover	0.28	0.49
		Soil Class	0.17	0.18
		Geology Class	0.22	0.22
Topography	0.14	Digital Elevation Model (DEM)	0.2	0.74
		Slope	0.25	1.11
		Topographic Wetness Index (TWI)	0.31	0.53
		Curvature	0.1	0.29
		Sediment Transport Index (STI)	0.16	0.28

The MDI algorithm is an inherent feature importance assessment method in the Random Forest framework [51,61], which quantifies the contribution of each input variable based on its ability to reduce node impurity during the construction of decision trees. In this approach, variables that provide greater improvement in the separation of flood and non-flood classes receive higher importance scores. The final importance of each criterion is calculated by averaging its contribution across all decision trees within the RF ensemble. Therefore, MDI provides an objective, data-driven evaluation of the relative influence of conditioning factors and helps identify the dominant variables controlling

flood susceptibility patterns in the study area. According to the Best-Worst method and the opinion of expert specialists, hydro-climatic, hydrological, land cover, and topographical criteria, respectively, are of greater importance. However, based on the RF model and the MDI algorithm, the 5 important criteria in flood zoning in the study area are: distance from rivers, slope, vegetation cover, cumulative flow, elevation, etc., which have played a significant role in this modeling.

5. Limitations and Future Research

Although the proposed framework demonstrates promising results in flood susceptibility mapping, several limitations should be acknowledged. First, uncertainties associated with expert-based weighting in the OWA-BWM approach remain an inherent limitation, as subjective judgments may introduce variability in the weighting process. Second, potential temporal inconsistencies among the multi-source datasets used in this study may influence model outputs. Third, the use of medium-resolution spatial datasets may limit the ability to capture fine-scale hydrological variability, particularly in complex terrain conditions. Finally, although independent validation was performed, more advanced validation strategies such as spatial cross-validation could further improve the robustness of the results.

Future research should focus on addressing these limitations by integrating higher-resolution datasets and downscaled hydro-climatic variables such as precipitation, evaporation, land surface temperature and soil moisture [62–67], which play a key role in runoff generation processes at the watershed scale. In addition, validation frameworks can be strengthened through the use of sensor-based observations, particularly Internet of Things (IoT)-enabled hydrological monitoring systems for real-time flood assessment [68–71].

Moreover, future studies should move toward hybrid and integrated modeling frameworks that combine machine learning and deep learning techniques to improve predictive accuracy and spatial generalization. A unified framework integrating both objective (data-driven) and subjective (expert-based) approaches could provide a more comprehensive decision-support system for flood risk assessment.

Finally, emerging concepts such as Digital Twin hydrological systems offer promising opportunities for real-time monitoring, simulation, and smart flood mapping. The integration of such technologies could significantly enhance dynamic flood prediction and support intelligent watershed management strategies.

6. Conclusions

Two different approaches to flood risk zoning, the OWA multi-criteria decision-making model and the RF data-driven model, were investigated and compared based on a comprehensive and precise analysis of flood risk assessment and representation at a regional scale. The results showed that the OWA model, with its adjustable ORness parameter, covered a wide range of decision-making scenarios from fully pessimistic to completely optimistic. This capability provides flexible sensitivity and uncertainty analysis. The RF model, on the other hand, offered more realistic predictions by focusing on complex patterns in historical data. Among the various OWA scenarios, the rational or neutral scenario (ORness = 50) showed the greatest consistency and closest agreement to the RF model results, serving as a suitable reference for scenario-based analyses and practical decision-making in flood risk management. This scenario created a suitable balance between optimism and pessimism and presented a reasonable distribution of risk classes. In contrast, scenarios with very low ORness tend to underestimate the risk, and scenarios with very high ORness tend to overestimate it, both of which could lead to incorrect or inefficient decisions in the risk management process. Finally, the findings of the current research highlighted

the potential of simultaneous and intelligent integration of judgment-based models like OWA and data-driven models like RF for flood risk management under complex and uncertain conditions.

Beyond methodological comparison, the results reveal a more fundamental implication regarding the epistemic nature of flood susceptibility modelling. The observed spatial discrepancies between OWA- and RF-derived outputs indicate that flood hazard representation is inherently model-dependent, emerging from the interaction between subjective weighting structures and data-driven statistical learning mechanisms. In this sense, susceptibility mapping should be interpreted as a conditional inference problem rather than a deterministic spatial prediction, where outputs are contingent upon the underlying decision logic, parameterization scheme, and learning strategy. The RF model captures latent multivariate dependencies through non-parametric learning, whereas OWA explicitly embeds decision-maker preference structures into the aggregation process, leading to structurally different risk surfaces even under identical input conditions. Therefore, the integration of both paradigms provides a dual-perspective framework that enhances epistemic robustness, improves uncertainty characterization, and supports more defensible decision-making under deep uncertainty in hydrological and watershed management systems.

Author Contributions: Conceptualization, M.R., B.M., M.K.F., R.K. and F.B.; methodology, M.R., B.M., M.K.F. and R.K.; software, M.R.; validation, M.K.F.; investigation, M.R. and M.K.F.; data curation, M.R.; writing—original draft preparation, M.R.; writing—review and editing, B.M., M.K.F., R.K. and F.B.; visualization, F.B. and M.R.; supervision, B.M. All authors have read and agreed to the published version of the manuscript.

Funding: This research received no external funding.

Data Availability Statement: The data used to support the findings of this study are available from the corresponding author upon reasonable request.

Acknowledgments: The authors used artificial intelligence (AI) tools to improve the English language, refine the translation of selected sections, and enhance the clarity and structure of the manuscript. All scientific content, interpretations, analyses, and conclusions were developed, verified, and approved by the authors, who assume full responsibility for the accuracy and integrity of the manuscript.

Conflicts of Interest: The authors declare no conflicts of interest.

References

1. Field, C.B. *Managing the Risks of Extreme Events and Disasters to Advance Climate Change Adaptation: Special Report of the Intergovernmental Panel on Climate Change*; Cambridge University Press: Cambridge, UK, 2012.
2. Rutgersson, A.; Kjellström, E.; Haapala, J.; Stendel, M.; Danilovich, I.; Drews, M.; Jylhä, K.; Kujala, P.; Larsén, X.G.; Halsnæs, K.; et al. Natural hazards and extreme events in the Baltic Sea region. *Earth Syst. Dyn. Discuss.* **2021**, *13*, 251–301. [CrossRef]
3. Rentschler, J.; Avner, P.; Marconcini, M.; Su, R.; Strano, E.; Vousdoukas, M.; Hallegatte, S. Global evidence of rapid urban growth in flood zones since 1985. *Nature* **2023**, *622*, 87–92. [CrossRef] [PubMed]
4. Alderman, K.; Turner, L.R.; Tong, S. Floods and human health: A systematic review. *Environ. Int.* **2012**, *47*, 37–47. [CrossRef]
5. Barbetta, S.; Coccia, G.; Moramarco, T.; Todini, E. Real-time flood forecasting downstream river confluences using a Bayesian approach. *J. Hydrol.* **2018**, *565*, 516–523. [CrossRef]
6. Li, Y.; Ryu, D.; Western, A.W.; Wang, Q.; Robertson, D.E.; Crow, W.T. An integrated error parameter estimation and lag-aware data assimilation scheme for real-time flood forecasting. *J. Hydrol.* **2014**, *519*, 2722–2736. [CrossRef]
7. Liu, Z.; Coleman, N.; Patrascu, F.I.; Yin, K.; Li, X.; Mostafavi, A. Artificial intelligence for flood risk management: A comprehensive state-of-the-art review and future directions. *Int. J. Disaster Risk Reduct.* **2024**, *117*, 105110.
8. Islam, T.; Zeleke, E.B.; Afroz, M.; Melesse, A.M. A Systematic Review of Urban Flood Susceptibility Mapping: Remote Sensing, Machine Learning, and Other Modeling Approaches. *Remote Sens.* **2025**, *17*, 524. [CrossRef]
9. Ratcliffe, H.; Kendig, A.; Vacek, S.; Carlson, D.; Ahlering, M.; Dee, L.E. Extreme precipitation promotes invasion in managed grasslands. *Ecology* **2024**, *105*, e4190. [PubMed]

10. Arnell, N.W.; Gosling, S.N. The impacts of climate change on river flood risk at the global scale. *Clim. Change* **2016**, *134*, 387–401. [CrossRef]
11. Tabari, H. Climate change impact on flood and extreme precipitation increases with water availability. *Sci. Rep.* **2020**, *10*, 13768. [CrossRef] [PubMed]
12. Eekhout, J.P.; Hunink, J.E.; Terink, W.; de Vente, J. Why increased extreme precipitation under climate change negatively affects water security. *Hydrol. Earth Syst. Sci.* **2018**, *22*, 5935–5946. [CrossRef]
13. Dobrovičová, S.; Dobrovič, R.; Dobrovič, J. The economic impact of floods and their importance in different regions of the world with emphasis on Europe. *Procedia Econ. Financ.* **2015**, *34*, 649–655. [CrossRef]
14. Fotovatikhah, F.; Herrera, M.; Shamshirband, S.; Ahmadi, M.; Ardabili, S.F.; Piran, J. Survey of computational intelligence as basis to big flood management: Challenges, research directions and future work. *Eng. Appl. Comput. Fluid Mech.* **2018**, *12*, 411–437. [CrossRef]
15. Goyal, H.R.; Ghanshala, K.K.; Sharma, S. Post flood management system based on smart IoT devices using AI approach. *Mater. Today Proc.* **2021**, *46*, 10411–10417. [CrossRef]
16. Paswan, N.G.; Ray, L.K. *Intelligent Solutions for Flood Management: Integrating Artificial Intelligence and Machine Learning, in Big Data, Artificial Intelligence, and Data Analytics in Climate Change Research: For Sustainable Development Goals*; Springer: Singapore, 2024; pp. 43–55.
17. Li, Z.; Zhou, Z.; Wang, H.; Li, X.; Shi, X.; Xiao, J.; Yang, Z.; Sun, M.; Li, X.; Jia, H. Artificial intelligence-incorporated prediction for urban flooding processes in the past 20 years: A critical review. *Environ. Model. Softw.* **2025**, *192*, 106525. [CrossRef]
18. Mudashiru, R.B.; Sabtu, N.; Abustan, I.; Balogun, W. Flood hazard mapping methods: A review. *J. Hydrol.* **2021**, *603*, 126846. [CrossRef]
19. Bentivoglio, R.; Isufi, E.; Jonkman, S.N.; Taormina, R. Deep learning methods for flood mapping: A review of existing applications and future research directions. *Hydrol. Earth Syst. Sci. Discuss.* **2022**, *26*, 4345–4378. [CrossRef]
20. Ashhar, M.; Keesara, V.R.; Sridhar, V. Flood inundation mapping of a river Stretch using machine learning algorithms in the Google Earth Engine environment. *J. Flood Risk Manag.* **2025**, *18*, e70062.
21. Liu, B.; Li, Y.; Ma, M.; Mao, B. A Comprehensive Review of Machine Learning Approaches for Flood Depth Estimation: Liu et al. Machine Learning Approaches for Flood Depth Estimation. *Int. J. Disaster Risk Sci.* **2025**, *16*, 433–445. [CrossRef]
22. Kordi-Karimabadi, F.; Fadaei-Kermani, E.; Ghaeini-Hessaroeyeh, M.; Farhadi, H. Integrating numerical models with deep learning techniques for flood risk assessment. *Sci. Rep.* **2025**, *15*, 8913. [PubMed]
23. Singha, C.; Sahoo, S.; Mahtaj, A.B.; Moghimi, A.; Welzel, M.; Govind, A. Advancing flood risk assessment: Multitemporal SAR-based flood inventory generation using transfer learning and hybrid fuzzy-AHP-machine learning for flood susceptibility mapping in the Mahananda River Basin. *J. Environ. Manag.* **2025**, *380*, 124972. [CrossRef]
24. Li, G.; Shao, W.; Su, X.; Li, Y.; Zhang, Y.; Song, T. Urban flood hazard assessment based on machine learning model. *Water Resour. Manag.* **2025**, *39*, 1953–1970. [CrossRef]
25. Saravanan, S.; Abijith, D.; Reddy, N.M.; Kss, P.; Janardhanam, N.; Sathiyamurthi, S.; Sivakumar, V. Flood susceptibility mapping using machine learning boosting algorithms techniques in Idukki district of Kerala India. *Urban Clim.* **2023**, *49*, 101503. [CrossRef]
26. Tanim, A.H.; McRae, C.B.; Tavakol-Davani, H.; Goharian, E. Flood detection in urban areas using satellite imagery and machine learning. *Water* **2022**, *14*, 1140. [CrossRef]
27. El Baida, M.; Hosni, M.; Boushaba, F.; Chourak, M. A systematic literature review on classification machine learning for urban flood hazard mapping. *Water Resour. Manag.* **2024**, *38*, 5823–5864. [CrossRef]
28. Singha, C.; Swain, K.C.; Meliho, M.; Abdo, H.G.; Almohamad, H.; Al-Mutiry, M. Spatial analysis of flood hazard zoning map using novel hybrid machine learning technique in Assam, India. *Remote Sens.* **2022**, *14*, 6229. [CrossRef]
29. Youssef, A.M.; Mahdi, A.M.; Pourghasemi, H.R. Landslides and flood multi-hazard assessment using machine learning techniques. *Bull. Eng. Geol. Environ.* **2022**, *81*, 370. [CrossRef]
30. El baida, M.; Boushaba, F.; Chourak, M.; Hosni, M.; Sabar, H. Classification machine learning models for urban flood hazard mapping: Case study of Zaio, NE Morocco. *Nat. Hazards* **2024**, *120*, 10013–10041. [CrossRef]
31. Islam, A.R.M.T.; Jibon, J.N.; Siddik, A.; Mallick, J.; Alqadhi, S.; Pal, S.C.; Purohit, S.; Senapathi, V. Predicting flood risks using advanced machine learning algorithms with a focus on Bangladesh: Influencing factors, gaps and future challenges. *Earth Sci. Inform.* **2025**, *18*, 300. [CrossRef]
32. Adeyemi, A.B.; Komolafe, A.A. Flood hazard zones prediction using machine-learning-based geospatial approach in lower niger river basin, Nigeria. *Nat. Hazards Res.* **2025**, *5*, 399–412. [CrossRef]
33. Wang, J.-H.; Lin, G.-F.; Huang, Y.-R.; Huang, I.-H.; Chen, C.-L. Application of hybrid machine learning model for flood hazard zoning assessments. *Stoch. Environ. Res. Risk Assess.* **2023**, *37*, 395–412. [CrossRef]
34. Singha, C.; Rana, V.K.; Pham, Q.B.; Nguyen, D.C.; Łupikasza, E. Integrating machine learning and geospatial data analysis for comprehensive flood hazard assessment. *Environ. Sci. Pollut. Res.* **2024**, *31*, 48497–48522. [CrossRef]

35. Andaryani, S.; Nourani, V.; Haghighi, A.T.; Keesstra, S. Integration of hard and soft supervised machine learning for flood susceptibility mapping. *J. Environ. Manag.* **2021**, *291*, 112731. [CrossRef]
36. Prasad, P.; Loveson, V.J.; Das, B.; Kotha, M. Novel ensemble machine learning models in flood susceptibility mapping. *Geocarto Int.* **2022**, *37*, 4571–4593.
37. Norallahi, M.; Seyed Kaboli, H. Urban flood hazard mapping using machine learning models: GARP, RF, MaxEnt and NB. *Nat. Hazards* **2021**, *106*, 119–137. [CrossRef]
38. Shikhteymour, S.R.; Borji, M.; Bagheri-Gavkosh, M.; Azimi, E.; Collins, T.W. A novel approach for assessing flood risk with machine learning and multi-criteria decision-making methods. *Appl. Geogr.* **2023**, *158*, 103035. [CrossRef]
39. Band, S.S.; Janizadeh, S.; Pal, S.C.; Saha, A.; Chakrabortty, R.; Melesse, A.M.; Mosavi, A. Flash flood susceptibility modeling using new approaches of hybrid and ensemble tree-based machine learning algorithms. *Remote Sens.* **2020**, *12*, 3568. [CrossRef]
40. Liu, Y.; Lu, X.; Yao, Y.; Wang, N.; Guo, Y.; Ji, C.; Xu, J. Mapping the risk zoning of storm flood disaster based on heterogeneous data and a machine learning algorithm in Xinjiang, China. *J. Flood Risk Manag.* **2021**, *14*, e12671. [CrossRef]
41. Chen, Y. Flood hazard zone mapping incorporating geographic information system (GIS) and multi-criteria analysis (MCA) techniques. *J. Hydrol.* **2022**, *612*, 128268. [CrossRef]
42. Mahmoody Vanolya, N.; Jelokhani-Niaraki, M. The use of subjective–objective weights in GIS-based multi-criteria decision analysis for flood hazard assessment: A case study in Mazandaran, Iran. *GeoJournal* **2021**, *86*, 379–398.
43. Khumaeroh, D.N.F.; Sari, D.N. Application of Analytical Hierarchy Process (AHP) and Geographic Information System (GIS) in flood hazard analysis in the Rawa Pening Sub-Watershed, Indonesia. *IOP Conf. Ser. Earth Environ. Sci.* **2024**, *1314*, 012114. [CrossRef]
44. Ghaffari Gilandeh, A.; Sobhani, B.; Ostadi, E. Combining Arc-GIS and OWA model in flooding potential analysis (case study: Meshkinshahr city). *Nat. Hazards* **2020**, *102*, 1435–1449. [CrossRef]
45. Tellman, B.; Sullivan, J.A.; Kuhn, C.; Kettner, A.J.; Doyle, C.S.; Brakenridge, G.R.; Erickson, T.A.; Slayback, D.A. Satellite imaging reveals increased proportion of population exposed to floods. *Nature* **2021**, *596*, 80–86. [CrossRef] [PubMed]
46. Rezaei, J. Best-worst multi-criteria decision-making method. *Omega* **2015**, *53*, 49–57. [CrossRef]
47. Rezaei, J. Best-worst multi-criteria decision-making method: Some properties and a linear model. *Omega* **2016**, *64*, 126–130. [CrossRef]
48. Yager, R.R. On ordered weighted averaging aggregation operators in multicriteria decisionmaking. *IEEE Trans. Syst. Man. Cybern.* **2002**, *18*, 183–190.
49. Yager, R.R. *On the Inclusion of Importances in OWA Aggregations, in The Ordered Weighted Averaging Operators: Theory and Applications*; Springer: Boston, MA, USA, 1997; pp. 41–59.
50. Malczewski, J.; Rinner, C. *Multicriteria Decision Analysis in Geographic Information Science*; Springer: New York, NY, USA, 2015; Volume 1.
51. Breiman, L. Random forests. *Mach. Learn.* **2001**, *45*, 5–32. [CrossRef]
52. Esfandiari, M.; Abdi, G.; Jabari, S.; McGrath, H.; Coleman, D. Flood hazard risk mapping using a pseudo supervised random forest. *Remote Sens.* **2020**, *12*, 3206. [CrossRef]
53. Ahmadianfar, I.; Ahmadianfar, I.; Asghar Heidari, A.; Noshadian, S.; Chen, H.; Gandomi, A.H. INFO: An efficient optimization algorithm based on weighted mean of vectors. *Expert Syst. Appl.* **2022**, *195*, 116516. [CrossRef]
54. Kiavarz, M.; Jelokhani-Niaraki, M. Geothermal prospectivity mapping using GIS-based Ordered Weighted Averaging approach: A case study in Japan's Akita and Iwate provinces. *Geothermics* **2017**, *70*, 295–304. [CrossRef]
55. Sajjadi, S.M.; Barihi, S.; Ahadiyan, J.; Nadian, H.A.; Valipour, M.; Bahmanpouri, F.; Khedri, P. Redesigning the fuse plug, emergency spillway, and flood warning system: An application of flood management. *Water* **2024**, *16*, 3694. [CrossRef]
56. Rahimi, M.; Malekmohammadi, B.; Firozjaei, M.K.; Kerachian, R.; Arsanjani, J.J.; Tan, M.L.; Awange, J.; Savic, D.; Duan, Q.; AghaKouchak, A. Integrating geospatial intelligence and machine learning for flood susceptibility mapping. *Sci. Rep.* **2026**, *16*, 10228. [CrossRef] [PubMed]
57. Kimuli, J.B.; Di, B.; Zhang, R.; Wu, S.; Li, J.; Yin, W. A multisource trend analysis of floods in Asia-Pacific 1990–2018: Implications for climate change in sustainable development goals. *Int. J. Disaster Risk Reduct.* **2021**, *59*, 102237. [CrossRef]
58. Mahmoodi, H.; Shorabeh, S.N.; Farhadi, M.; Rahimi, M.; Firozjaei, M.K. National-scale spatial modelling of dust storm pollution and vulnerability of tourism destinations and infrastructure. *Sci. Rep.* **2026**, *16*, 15844. [CrossRef] [PubMed]
59. Rahimi, M.; Jalali, M.; Zolghadr-Asli, B.; AghaKouchak, A.; Mirchi, A. Water Governance and Policymaking in Iran Over the Last Half-Century: Inefficiencies and Shortcomings. In *EGU General Assembly Conference Abstracts, Proceedings of the European Geosciences Union General Assembly, Vienna, Austria, 27 April–2 May 2025*; European Geosciences Union (EGU): Munich, Germany, 2025.
60. Mansour, M.M.; Ibrahim, M.G.; Fujii, M.; Nasr, M. Sustainable development goals (SDGs) associated with flash flood hazard mapping and management measures through morphometric evaluation. *Geocarto Int.* **2022**, *37*, 11116–11133. [CrossRef]
61. Strobl, C.; Boulesteix, A.-L.; Zeileis, A.; Hothorn, T. Bias in random forest variable importance measures: Illustrations, sources and a solution. *BMC Bioinform.* **2007**, *8*, 25. [CrossRef]

62. Karimi Firozjaei, M.; Rahimi, M.; Kiavarz, M.; Rahimi, L.; AghaKouchak, A.; De Michele, C.; Manfreda, S. Enhancing Spatial Resolution and Accuracy of Land Surface Temperature: Integration of Regression-based and Surface Energy Balance Models. In *EGU General Assembly Conference Abstracts, Proceedings of the European Geosciences Union General Assembly, Vienna, Austria, 27 April–2 May 2025*; European Geosciences Union (EGU): Munich, Germany, 2025.
63. Rahimi, M.; Parsaie, A. Estimation of evapotranspiration using machine learning models. *Preprints* **2024**.
64. Yang, T.; Li, H.; Wang, W.; Xu, C.; Yu, Z. Statistical downscaling of extreme daily precipitation, evaporation, and temperature and construction of future scenarios. *Hydrol. Process.* **2012**, *26*, 3510–3523. [CrossRef]
65. Zhang, D.; Zhang, M.; Chen, J.; Ge, Y. Soil moisture downscaling using machine learning with scale-aware, physically informed feature constraints. *Soil Adv.* **2025**, *5*, 100096. [CrossRef]
66. Jian, J.; He, S.; Liu, W.; Liu, S.; Guo, L. A refined method for the simulation of catchment rainfall–runoff based on satellite–precipitation downscaling. *J. Hydrol.* **2025**, *653*, 132795. [CrossRef]
67. Zhu, H.; Zhou, Q.; Krisp, J.M. Exploring machine learning approaches for precipitation downscaling. *Geo-Spat. Inf. Sci.* **2025**, *28*, 2673–2689. [CrossRef]
68. Malekmohammadi, B.; Rahimi, M.; Kerachian, R.; Singh, V.P.; Falconer, R.A.; Noori, R.; Bahmanpouri, F. An Approach for IoT-Based Smart Sensors Placement in Urban Water Networks Under Natural Hazards. In *EGU General Assembly Conference Abstracts, Proceedings of the European Geosciences Union General Assembly, Vienna, Austria, 27 April–2 May 2025*; European Geosciences Union (EGU): Munich, Germany, 2025.
69. Binti Zahir, S.; Ehkan, P.; Sabapathy, T.; Jusoh, M.; Osman, M.N.; Yasin, M.N.; Wahab, Y.A.; Hambali, N.; Ali, N.; Bakhit, A.; et al. Smart IoT flood monitoring system. *J. Phys. Conf. Ser.* **2019**, *1339*, 012043. [CrossRef]
70. Zakaria, M.I.; Jabbar, W.A.; Sulaiman, N. Development of a smart sensing unit for LoRaWAN-based IoT flood monitoring and warning system in catchment areas. *Internet Things Cyber-Phys. Syst.* **2023**, *3*, 249–261. [CrossRef]
71. Elkhodr, M.; Al-Sabbagh, A. An integrative framework for flood monitoring and water quality management enabled by emerging IoT, drone, blockchain, and AI technologies. *Clust. Comput.* **2026**, *29*, 97. [CrossRef]

Disclaimer/Publisher's Note: The statements, opinions and data contained in all publications are solely those of the individual author(s) and contributor(s) and not of MDPI and/or the editor(s). MDPI and/or the editor(s) disclaim responsibility for any injury to people or property resulting from any ideas, methods, instructions or products referred to in the content.